Communications in Nonlinear Science and Numerical Simulation 106 (2022) 106099

Contents lists available at ScienceDirect

Communications in Nonlinear Science and Numerical Simulation

journal homepage: www.elsevier.com/locate/cnsns

KAM quasi-periodic tori for the dissipative spin–orbit problem☆

Renato Calleja [a], Alessandra Celletti [b], Joan Gimeno [b,*], Rafael de la Llave [c]

[a] Department of Mathematics and Mechanics, IIMAS, National Autonomous University of Mexico (UNAM), Apdo. Postal 20-126, C.P. 045L0, Mexico D.F., Mexico
[b] Department of Mathematics, University of Rome Tor Vergata, Via della Ricerca Scientifica 1, 00133 Rome, Italy
[c] School of Mathematics, Georgia Institute of Technology, 686 Cherry St., Atlanta GA 30332-0160, USA

ARTICLE INFO

Article history:
Available online 6 November 2021

Keywords:
KAM theory
Conformally symplectic systems
Dissipative spin–orbit problem
Quasi-periodic attractors

ABSTRACT

We provide evidence of the existence of KAM quasi-periodic attractors for a dissipative model in Celestial Mechanics. We compute the attractors extremely close to the breakdown threshold.

We consider the spin–orbit problem describing the motion of a triaxial satellite around a central planet under the simplifying assumption that the center of mass of the satellite moves on a Keplerian orbit, the spin-axis is perpendicular to the orbit plane and coincides with the shortest physical axis. We also assume that the satellite is non-rigid; as a consequence, the problem is affected by a dissipative tidal torque that can be modeled as a time-dependent friction, which depends linearly upon the velocity.

Our goal is to fix a frequency and compute the embedding of a smooth attractor with this frequency. This task requires to adjust a drift parameter.

We have shown in Calleja et al. (2020) that it is numerically efficient to study Poincaré maps; the resulting *spin–orbit map* is conformally symplectic, namely it transforms the symplectic form into a multiple of itself. In Calleja et al. (2020), we have developed an extremely efficient (quadratically convergent, low storage requirements and low operation count per step) algorithm to construct quasi-periodic solutions and we have implemented it in extended precision. Furthermore, in Calleja et al. (2020) we have provided an "a-posteriori" KAM theorem that shows that if we have an embedding and a drift parameter that satisfy the invariance equation up to an error which is small enough with respect to some explicit condition numbers, then there is a true solution of the invariance equation. This a-posteriori result is based on a Nash–Moser hard implicit function theorem, since the Newton method incurs losses of derivatives.

The goal of this paper is to provide numerical calculations of the condition numbers and verify that, when they are applied to the numerical solutions, they will lead to the existence of the torus for values of the parameters extremely close to the parameters of breakdown. Computing reliably close to the breakdown allows to discover several interesting phenomena, which we will report in Calleja et al. (2020).

☆ R.C. was partially supported by UNAM-DGAPA PAPIIT Project IN 101020. A.C. was partially supported by the MIUR Excellence Department Project awarded to the Department of Mathematics, University of Rome Tor Vergata, CUP E83C18000100006, EU H2020 MSCA ETN Stardust-Reloaded Grant Agreement 813644, and with J.G. by MIUR-PRIN 20178CJA2B "New Frontiers of Celestial Mechanics: theory and Applications". J.G. has also been supported by the Spanish grant PGC2018-100699-B-I00 (MCIU/AEI/FEDER, UE) and the Catalan grant 2017 SGR 1374. J.G. thanks the School of Mathematics of GT for its hospitality in Spring 2019 and Fall 2019. R.L. has been partially supported by NSF grant DMS 1800241.

* Corresponding author.
E-mail addresses: calleja@mym.iimas.unam.mx (R. Calleja), celletti@mat.uniroma2.it (A. Celletti), joan@maia.ub.es (J. Gimeno), rafael.delallave@math.gatech.edu (R. de la Llave).

https://doi.org/10.1016/j.cnsns.2021.106099
1007-5704/© 2021 Elsevier B.V. All rights reserved.

The numerical calculations of the condition numbers presented here are not completely rigorous, since we do not use interval arithmetic to estimate the round off error and we do not estimate rigorously the truncation error, but we implement the usual standards in numerical analysis (using extended precision, checking that the results are not affected by the level of precision, truncation, etc.). Hence, we do not claim a computer-assisted proof, but the verification is more convincing than a standard numerics. We hope that our work could stimulate a computer-assisted proof.
© 2021 Elsevier B.V. All rights reserved.

1. Introduction

Kolmogorov–Arnold–Moser (hereafter KAM) theory [1–3] concerns the existence of quasi-periodic motions in non-integrable dynamical systems. In its original formulation, it was applied to nearly-integrable Hamiltonian systems.

An important recent development is the *a-posteriori KAM theory* (see [4,5]) that does not require that the system is close to integrable, but rather that there is an approximate solution of an invariance equation that satisfies some non-degeneracy conditions. Given an a-posteriori KAM theorem, one does not need to justify the way that the approximate solution is constructed (it could be done by formal expansions or just by numerical tries), but one must provide rigorous estimates on the error of the invariance equation and the condition numbers involved in the theorem statement.

The KAM theory has been extended to general systems (see, e.g., [6]). This theory fixes the frequency of the quasi-periodic orbit searched, but adjusting parameters in the system. This general KAM theory is even more effective if the system preserves some geometric structures [7–9]. From the mathematical point of view, the number of parameters to adjust may be reduced (e.g., in the Hamiltonian case, there are no parameters to be adjusted). Numerically, one can use identities coming from the geometry to develop fast algorithms that also require small storage space and enjoy good stability properties. For the purposes of our paper, the most relevant development is [10], which established an a-posteriori KAM theorem and presented efficient numerical algorithms for *conformally symplectic systems* (that is, systems that transform the symplectic form into a multiple of itself). Conformally symplectic systems appear in a variety of applications, including Euler–Lagrange equations of exponentially discounted Lagrangians, thermostats, etc.

The goal of this paper is to study the applicability of a-posteriori KAM theory for a specific model of Celestial Mechanics known as the *spin–orbit problem with tidal torque*. This model describes the rotational motion of a non-rigid triaxial ellipsoid orbiting around a point-mass planet. We assume that the planet moves in a Keplerian orbit, the rotation axis is perpendicular to the orbital plane and aligned with the shortest physical axis of the satellite. Furthermore, we assume that the system experiences a tidal force proportional to the velocity, which makes it into a conformally symplectic system. This model has been studied in [11–13].

Efficient numerical methods to find quasi-periodic orbits in the spin–orbit model were implemented in [14]. Taking advantage of the extreme efficiency of the methods, modern programming tools and the power of modern hardware, the calculations of [14] were run in high precision and produced the parameterization of quasi-periodic orbits and adjusted parameters that solve the invariance equations with very high accuracy, even very close to the breakdown[1].

The goal of this paper is to study the application of the a-posteriori theorem in [10] to the calculations in [14]. We take the calculations in [14], and evaluate numerically the condition numbers required in [10]. Similar results for an explicitly given mapping appear in [15]. In the present problem, the map considered is not given by an explicit formula, but is obtained by integrating an ordinary differential equation. This requires new analysis and numerical studies of the variational equations.

The results presented here come short of a full computer-assisted proof, since the evaluation of the error and the condition numbers are not completely rigorous. We do not take into account round-off or truncation errors.

We certainly hope that the present effort could serve as inspiration for others to close the gap and provide a true computer-assisted proof and, needless to say, we would be happy to provide detailed data and encouragement. Even if not the final word on existence, we think that the work presented goes beyond the regular standards of numerical computations and is a significant progress in the area of the computations of tori, even close to the breakdown. We think that it is rather remarkable that the algorithms inspired by the theory are also the most efficient ones.

Computing close to the breakdown and being able to trust the computation is not just an affectation, but uncovers new phenomena that present a challenge to mathematics.

[1] As a matter of fact, there is no alternative numerical method that can compute as close to the breakdown, so that the estimates of this paper are the best estimates for the threshold, since the solutions we can compute have all the signs of being very deteriorated.

We note that, even if the computation is doable, but delicate for values of the perturbation close to the threshold, it remains extremely reliable and easy for many values of astronomical interest, so that KAM theory and their algorithms become a relevant tool to astronomers, overcoming the concerns – relevant at the time they were written – of [16].

This paper is organized as follows. The equation of motion describing the dissipative spin–orbit problem is shortly recalled in Section 2. We study the Poincaré map associated to such a model in Section 3; in this way we obtain a *spin–orbit map*, which is conformally symplectic, and we compute the corresponding conformally symplectic factor, which is the term by which the symplectic form gets multiplied, when the map is applied to the symplectic form. Then, we use the KAM theorem for conformally symplectic maps formulated in [15] (see Section 4). Contrary to the implementation to the standard map, the application of the theorem to the spin–orbit problem is more complex and it requires a careful computation of some constants as described in Section 5. This procedure leads to the final results that we present in Section 6 for two different frequencies: the golden ratio and a second frequency between one and the golden ratio.

2. The spin–orbit problem with tidal torque

For the sake of motivation, in this section we present the physical basis of the model considered. Even if this motivates the questions asked, it is logically independent of the analysis.

Consider the motion of a non-rigid satellite $\mathcal{S}$ that we assume to have a triaxial shape and principal moments of inertia $\mathcal{A} < \mathcal{B} < \mathcal{C}$. We assume that the barycenter of the satellite $\mathcal{S}$ moves on an elliptic Keplerian orbit with semimajor axis a, eccentricity e, and with the planet $\mathcal{P}$ in one focus. The satellite rotates around the smallest physical axis, in such a way that the spin-axis is perpendicular to the orbit plane (see, e.g., [17–21]).

We normalize the units of measure of time so that the orbital period T_{orb} is equal to 2π, which implies that the mean motion is $n = 2\pi/T_{orb} = 1$; we introduce the *perturbative parameter* ε, which measures the equatorial ellipticity of the satellite:

$$\varepsilon := \frac{3}{2}\frac{\mathcal{B}-\mathcal{A}}{\mathcal{C}} \,. \tag{1}$$

We denote by x the angle between the largest physical axis of the triaxial satellite and the periapsis line. The equation of motion of the spin–orbit problem, using the formulation in [22,23] for the tidal torque, is given by

$$\frac{d^2x(t)}{dt^2} + \varepsilon\left(\frac{a}{r(t)}\right)^3 \sin\big(2x(t) - 2f(t)\big) = -\eta\left(\frac{a}{r(t)}\right)^6 \left(\frac{dx(t)}{dt} - \frac{df(t)}{dt}\right) , \tag{2}$$

where $r(t) = r(t;e)$ and $f(t) = f(t;e)$ are the orbital radius and the true anomaly of the Keplerian ellipse, and $\eta > 0$ is the *dissipative constant* depending on the physical features of the satellite. Denoting by u the eccentric anomaly, then

$$r = a(1 - e\cos u) \,, \qquad \tan\left(\frac{f}{2}\right) = \sqrt{\frac{1+e}{1-e}}\tan\left(\frac{u}{2}\right) .$$

For $\eta = 0$ the model becomes conservative and takes a nearly-integrable form with ε being the *perturbing parameter*. We also introduce the spin–orbit problem with tidal torque *averaged* over one orbital period (see, e.g., [14,23]) as given by the equation

$$\frac{d^2x(t)}{dt^2} + \varepsilon\left(\frac{a}{r(t)}\right)^3 \sin\big(2x(t) - 2f(t)\big) = -\eta\bar{L}(e)\left(\frac{dx(t)}{dt} - \frac{\bar{N}(e)}{\bar{L}(e)}\right) , \tag{3}$$

where

$$\bar{L}(e) := \frac{1}{(1-e^2)^{9/2}}\left(1 + 3e^2 + \frac{3}{8}e^4\right) ,$$
$$\bar{N}(e) := \frac{1}{(1-e^2)^{6}}\left(1 + \frac{15}{2}e^2 + \frac{45}{8}e^4 + \frac{5}{16}e^6\right) .$$

3. The conformally symplectic spin–orbit map

Following [14], we introduce a discrete system, which is obtained by computing the Poincaré map P_e associated to (2). Precisely, setting $y = \dot{x}$, we can write the map as

$$P_e(x_0, y_0; \varepsilon) := \begin{pmatrix} x(2\pi; x_0, y_0, \varepsilon) \\ y(2\pi; x_0, y_0, \varepsilon) \end{pmatrix} \,, \tag{4}$$

where $x(2\pi; x_0, y_0, \varepsilon)$ and $y(2\pi; x_0, y_0, \varepsilon)$ denote the solution of (2) at time $t = 2\pi$ with initial conditions (x_0, y_0) at $t = 0$. Writing P_e in components, say $P_e \equiv (P_e^{(1)}, P_e^{(2)})$, the *spin–orbit Poincaré map* becomes:

$$\begin{aligned} \bar{x} &= P_e^{(1)}(x, y; \varepsilon) \,, \\ \bar{y} &= P_e^{(2)}(x, y; \varepsilon) \,. \end{aligned} \tag{5}$$

For numerical reasons, it is better to consider the change of coordinates

$$\Psi_e := 2\pi \begin{pmatrix} 1 & 0 \\ 0 & 1-e \end{pmatrix} \tag{6}$$

and define the map $G_e := \Psi_e \circ P_e \circ \Psi_e^{-1}$ which can be computed accurately by numerical integrators such as [24,25].

The map (5), equivalently G_e, inherits several properties of the continuous system (2). In particular, the map is *conformally symplectic*, which means that it transforms the symplectic form into a multiple of itself, according to the following definition.

Definition 3.1. Let $\mathcal{M} = \mathbb{T}^n \times U$ with $U \subseteq \mathbb{R}^n$ an open and simply connected domain with smooth boundary. We endow $\mathcal{M}$ with a symplectic form Ω. A diffeomorphism $f : \mathcal{M} \to \mathcal{M}$ is conformally symplectic, if there exists a function $\lambda : \mathcal{M} \to \mathbb{R}$ such that

$$f^*\Omega = \lambda\Omega \ , \tag{7}$$

where f^* denotes the pull–back of f.

We will call λ the conformal factor. For $\lambda = 1$ we have a symplectic diffeomorphism. In the following, we will consider the family $P_e : \mathcal{M} \to \mathcal{M}$, defined in (4), of diffeomorphisms depending on a parameter $e \in [0, 1)$ to which we refer as the *drift parameter*. In this case (7) is replaced by

$$P_e^*\Omega = \lambda\Omega \ . \tag{8}$$

The definition of conformally symplectic continuous systems is given as follows.

Definition 3.2. A vector field X is a conformally symplectic flow if, denoting by L_X the Lie derivative, there exists a function $\lambda : \mathbb{R}^{2n} \to \mathbb{R}$ such that

$$L_X\Omega = \lambda\Omega \ . \tag{9}$$

If Φ_t denotes the flow at time t, then (9) implies that

$$(\Phi_t)^*\Omega = \exp(\lambda t)\Omega \ .$$

The dissipative spin–orbit model (2) is an example of a conformally symplectic vector field. An important result for our purposes is that the Poincaré map associated to a conformally symplectic vector field is a conformally symplectic map. As a consequence, the spin–orbit Poincaré map defined in (5) is conformally symplectic with the conformally symplectic factor given by

$$\lambda(x, y) = \sigma |\det DP_e(x, y; \varepsilon)|, \qquad \sigma = \pm 1 \ , \tag{10}$$

where σ denotes the orientation of P_e.

As shown in [14], the conformal factor is given explicitly in terms of the orbital eccentricity and the dissipative parameter:

$$\lambda = \exp\left(-\eta\pi \frac{3e^4 + 24e^2 + 8}{4\left(1 - e^2\right)^{9/2}} \right) . \tag{11}$$

When $\eta > 0$ we have a contractive system, if $\eta < 0$ we have an expansive system and if $\eta = 0$ we have a symplectic system. In the following we will just consider the contractive case with $\eta > 0$.

4. KAM theorem and invariant attractors

The statement of the KAM theorem that we will apply to the spin–orbit problem requires a set of preliminary notations and notions. We start to give, in Section 4.1, the definition of the norms and some results on Cauchy estimates on the derivatives. In Section 4.2 we give the definition of Diophantine frequency and we present some results on the solution of the cohomology equation. The definition of KAM attractor and the invariance equation to be satisfied is given in Section 4.3. Finally, the statement of the KAM theorem, borrowed from [15], is given in Section 4.4.

4.1. Norms and Cauchy estimates

The norm of a vector $\underline{v} = \left(\begin{smallmatrix} v_1 \\ v_2 \end{smallmatrix}\right) \in \mathbb{R}^2$ is defined as

$$\|\underline{v}\| := |v_1| + |v_2| \ .$$

The norm of a matrix $A = \left(\begin{smallmatrix} a_{11} & a_{12} \\ a_{21} & a_{22} \end{smallmatrix}\right) \in \mathbb{R}^2 \times \mathbb{R}^2$ is defined as

$$\|A\| := \max\left\{ |a_{11}| + |a_{21}|, \ |a_{12}| + |a_{22}| \right\} \ .$$

Next, we consider the norm of functions and vector functions. To this end, for $\rho > 0$ we introduce the complex extensions of a torus $\mathbb{T}$, a set B and the manifold $\mathcal{M} = \mathbb{T} \times B$ as

$$\begin{aligned} \mathbb{T}_\rho &:= \{x + \mathrm{i}y \in \mathbb{C}/\mathbb{Z} \colon x \in \mathbb{T}\ ,\ |y| \le \rho\}\ , \\ B_\rho &:= \{x + \mathrm{i}y \in \mathbb{C} \colon x \in B\ ,\quad |y| \le \rho\}\ , \\ \mathcal{M}_\rho &:= \mathbb{T}_\rho \times B_\rho\ . \end{aligned} \tag{12}$$

By $\mathcal{A}_\rho$ we denote the set of functions analytic in the interior of $\mathbb{T}_\rho$ and extending continuously to the boundary of $\mathbb{T}_\rho$. This set is endowed with the norm

$$\|f\|_\rho := \sup_{z \in \mathbb{T}_\rho} |f(z)|\ . \tag{13}$$

Similarly, for a vector valued function $f = (f_1, f_2, \dots, f_n)$, $n \ge 1$, we define the norm $\|f\|_\rho := \sup_{z\in\mathbb{T}\rho} (|f_1(z)| + \cdots + |f_n(z)|)$ that we bound as

$$\|f\|_\rho \le \|f_1\|_\rho + \|f_2\|_\rho + \cdots + \|f_n\|_\rho\ . \tag{14}$$

If F denotes an $n_1 \times n_2$ matrix valued function, then we define its norm for columns as $\|F\|_\rho := \sup_{z\in\mathbb{T}_\rho} |F(z)|$ that we bound as

$$\|F\|_\rho \le \max\left\{ \sum_{i=1}^{n_1} \sup_{z\in\mathbb{T}_\rho} |F_{i1}(z)|, \dots, \sum_{i=1}^{n_1} \sup_{z\in\mathbb{T}_\rho} |F_{in_2}(z)| \right\}. \tag{15}$$

The following classical lemma gives a bound on the derivatives on smaller domains than the initial function (see, e.g., [15] for its proof).

Lemma 4.1. *Given a function $h \in \mathcal{A}_\rho$, its first derivative can be bounded as*

$$\|Dh\|_{\rho-\delta} \le \delta^{-1}\ \|h\|_\rho\ , \tag{16}$$

where $0 < \delta < \rho$.

4.2. Diophantine frequency and the cohomology equation

One of the main assumptions in KAM theory is that the frequency satisfies a Diophantine assumption that, in view of the application of KAM theory to the spin–orbit map (5), we introduce as follows.

Definition 4.2. Let $\omega \in \mathbb{R}$ and let $\tau \ge 1$, $\nu > 0$. The number ω is said Diophantine of class τ and constant ν, $\omega \in \mathcal{D}(\nu, \tau)$, if for all $q \in \mathbb{Z}$ and $k \in \mathbb{Z}\backslash\{0\}$, it satisfies the following inequality

$$|\omega k - q|\ \ge\ \nu |k|^{-\tau}\ . \tag{17}$$

Another important ingredient at the basis of the proof of the KAM theorem is the solution of a cohomology equation of the form

$$\varphi(\theta + \omega) - \lambda\varphi(\theta) = \vartheta(\theta)\ , \tag{18}$$

where $\theta \in \mathbb{T}$ and ϑ is a Lebesgue measurable function.

The following lemmas yield the existence of a solution of (18) given by a Lebesgue measurable function φ. The first result, Lemma 4.3, is valid when $|\lambda| \ne 1$ and $\omega \in \mathbb{R}$. It gives an estimate on the solution which depends on λ and indeed explodes as $|\lambda|$ tends to 1. The second result, Lemma 4.4, is valid for any λ and Diophantine frequency ω. It provides a uniform estimate of the solution. We refer to [10,15] for the proofs of Lemmas 4.3 and 4.4.

In [10], one can find also estimates that are uniform for $\lambda \in [A^{-1}, A]$ for $A > 1$ and, hence allow to study the (singular) limit of zero dissipation. These estimates are very similar to the estimates in Lemma 4.4 (they use the Diophantine condition and they entail a loss of domain).

Lemma 4.3. *Let $|\lambda| \ne 1$ and $\omega \in \mathbb{R}$. Given any Lebesgue measurable function ϑ, there exists a Lebesgue measurable function φ which satisfies (18) and which is bounded by*

$$\|\varphi\|_\rho \le \big|\,|\lambda| - 1\,\big|^{-1} \|\vartheta\|_\rho\ .$$

The derivatives of φ with respect to λ are bounded by

$$\|D_\lambda^j \varphi\|_\rho \le \frac{j!}{\big|\,|\lambda| - 1\,\big|^{j+1}}\ \|\vartheta\|_\rho\ , \qquad j \ge 1\ .$$

Lemma 4.4. *Assume that $\lambda \in [A_0, A_0^{-1}]$ for some $0 < A_0 < 1$ in (18) and let $\omega \in \mathcal{D}(\nu, \tau)$. Let $\vartheta \in \mathcal{A}_\rho$, $\rho > 0$, be a function such that*

$$\int_{\mathbb{T}} \vartheta(\theta)\, d\theta = 0 \ .$$

Then, there exists one, and only one, solution of (18) with zero average:

$$\int_{\mathbb{T}} \varphi(\theta)\, d\theta = 0 \ .$$

Moreover, if $\varphi \in \mathcal{A}_{\rho-\delta}$ for $0 < \delta < \rho$, then we have

$$\|\varphi\|_{\rho-\delta} \le C_0\ \nu^{-1}\ \delta^{-\tau} \|\vartheta\|_\rho \ , \tag{19}$$

where

$$C_0 = \frac{1}{(2\pi)^\tau}\ \frac{\pi}{2^\tau(1+\lambda)} \sqrt{\frac{\Gamma(2\tau+1)}{3}} \tag{20}$$

and Γ denotes the gamma function.

We remark that [26] provides a better estimate for the constant C_0 in the symplectic case. Its expression is more complicated than (20). However, for our parameter values, it seems that the estimate (20) suffices to reach the final result of getting analytic estimates close to the break-down.

4.3. KAM attractor and the invariance equation

In this Section, we introduce the definition of a KAM attractor with Diophantine frequency ω for a family f_e of conformally symplectic maps. We call e the drift parameter, since we recognize that the drift is related to the eccentricity, although the drift might in principle coincide with a different parameter. This will require to satisfy the invariance Eq. (21) below, which will be the centerpiece of the KAM theorem of Section 4.4.

Definition 4.5. Let $f_e : \mathcal{M} \to \mathcal{M}$ be a family of conformally symplectic maps. A KAM attractor with frequency ω is an invariant torus which is described by an embedding $K : \mathbb{T} \to \mathcal{M}$ and a drift parameter e, which satisfy the following invariance equation for $\theta \in \mathbb{T}$:

$$f_e \circ K(\theta) = K(\theta + \omega) \ . \tag{21}$$

We remark that solving Eq. (21) will require to determine both K and e.

Denoting by T_ω the shift by ω such that for a function K, we have $(K \circ T_\omega)(\theta) = K(\theta + \omega)$, then the invariance equation (21) can be written as

$$f_e \circ K = K \circ T_\omega \ .$$

4.4. The KAM theorem

The KAM statement provided in [15] applies to two-dimensional maps and, although it has been applied to the dissipative standard map, the formulation of the KAM theorem was given for a general system. Therefore, we can apply the main theorem stated in [15] to the Poincaré map of the spin–orbit problem (2).

The KAM theorem in [15] gives explicit conditions that ensure that, given an approximate solution, there is a true solution. This requires the computation of several constants that we list in Appendix A to make the paper self contained. If the map was given by an explicit formula (as it was the case in [15]) some of the constants can be obtained using calculus. In our case, since the map is obtained integrating an ODE, we obtain the estimates integrating the equation in a complex domain.

Having fixed a Diophantine frequency ω and after computing the value of the conformal factor λ, we look for an embedding K and a drift parameter e which satisfy the invariance equation (21). The solution can be obtained under a non-degeneracy condition (see H3 in Theorem 4.6).

In the spin–orbit problem, the description of the computation of the solution is given in Section 4.6, while the verification of the KAM conditions is provided in Section 6.

Let us assume that we start with an approximate solution (K_0, e_0) which satisfies the invariance Eq. (21) up to an error term E_0, that is,

$$E_0(\theta) = f_{e_0} \circ K_0(\theta) - K_0(\theta + \omega) \ . \tag{22}$$

Before stating the main theorem, we need to introduce the following auxiliary quantities:

$$\begin{aligned} N_0(\theta) &:= (DK_0(\theta)^\top DK_0(\theta))^{-1} , \\ M_0(\theta) &:= [DK_0(\theta) \mid J^{-1} \circ K_0(\theta)\, DK_0(\theta) N_0(\theta)] , \\ S_0(\theta) &:= ((DK_0 N_0) \circ T_\omega)^\top (\theta) Df_{e_0} \circ K_0(\theta) J^{-1} \circ K_0(\theta) DK_0(\theta) N_0(\theta) , \end{aligned} \tag{23}$$

where the superscript $\top$ denotes transposition and the matrix J is the matrix representation of the symplectic form,

$$\Omega_z(u, v) = \langle u, J(z)v \rangle,$$

with $z \in \mathcal{M}$. For the applications we have in mind, J is constant and it is defined as

$$J = \begin{pmatrix} 0 & 1 \\ -1 & 0 \end{pmatrix} . \tag{24}$$

Theorem 4.6 is a constructive version of Theorem 20 in [10] and it applies to mapping systems, like the Poincaré map P_e defined in (4) associated to (2). In this case the conformal factor λ only depends on the dissipation η and the eccentricity e, and the map P_e depends on the three parameter η, ε, and e.

Theorem 4.6. *Let Λ be an open subset of $\mathbb{R}$ and for all $e \in \Lambda$, let $f_e : \mathcal{M} \to \mathcal{M}$ be a conformally symplectic map defined on the manifold $\mathcal{M} = B \times \mathbb{T}$; here $B \subset \mathbb{R}$ denotes an open and simply connected domain with smooth boundary. Assume that f_e is analytic on an open connected domain $\mathcal{C} \subset \mathbb{C} \times \mathbb{C}/\mathbb{Z}$. Assume the following hypotheses.*

H1. *The frequency ω is Diophantine as in (17), namely $\omega \in \mathcal{D}(\nu, \tau)$.*

H2. *The approximate solution (K_0, e_0), $K_0 \in \mathcal{A}_{\rho_0}$ for some $\rho_0 > 0$ and $e_0 \in \Lambda$, satisfies (21) up to an error function $E_0 = E_0(\theta)$ as in (22). We denote by ε_0 the size of the error function, that is,*

$$\varepsilon_0 := \|E_0\|_{\rho_0} .$$

H3. *Assume that the following non-degeneracy condition is fulfilled:*

$$\det \begin{pmatrix} \overline{S}_0 & \overline{S_0 (B_{b0})^0} + \overline{\widetilde{A}_0^{(1)}} \\ \lambda - 1 & \overline{\widetilde{A}_0^{(2)}} \end{pmatrix} \neq 0 ,$$

where S_0 is defined in (23), $\widetilde{A}_0^{(1)}$, $\widetilde{A}_0^{(2)}$ are the first and second elements of

$$\widetilde{A}_0 = M_0^{-1} \circ T_\omega D_e f_{e_0} \circ K_0 ,$$

$(B_{b0})^0$ is the solution (with zero average in the $\lambda = 1$ case) of the equation

$$\lambda (B_{b0})^0 - (B_{b0})^0 \circ T_\omega = -(\widetilde{A}_0^{(2)})^0 ,$$

and $(\widetilde{A}_0^{(2)})^0$ is the zero average part of $\widetilde{A}_0^{(2)}$.
Then, let $\mathcal{T}_0$ be the twist constant *defined as*

$$\mathcal{T}_0 := \left\| \begin{pmatrix} \overline{S}_0 & \overline{S_0 (B_{b0})^0} + \overline{\widetilde{A}_0^{(1)}} \\ \lambda - 1 & \overline{\widetilde{A}_0^{(2)}} \end{pmatrix}^{-1} \right\| .$$

H4. *Assume that for some $\zeta > 0$ we have*

$$\operatorname{dist}(e_0, \partial\Lambda) \geq \zeta , \qquad \operatorname{dist}(K_0(\mathbb{T}_{\rho_0}), \partial\mathcal{C}) \geq \zeta .$$

H5. *Let δ_0 be such that $0 < \delta_0 < \rho_0$. Introduce the quantity $\kappa_e := 4C_{\sigma 0}$ with $C_{\sigma 0}$ constant (see Appendix A). Define the quantities*

$$
\begin{aligned}
Q_z &:= \sup_{z\in\mathcal{C}} |Df_{e_0}(z)| \ , \\
Q_e &:= \sup_{z\in\mathcal{C},e\in\Lambda,|e-e_0|<2\kappa_e\varepsilon_0} |D_e f_e(z)| \ , \\
Q_{zz} &:= \sup_{z\in\mathcal{C}} |D^2 f_{e_0}(z)| \ , \\
Q_{ez} &:= \sup_{z\in\mathcal{C}} |DD_e f_{e_0}(z)| \ , \\
Q_{zzz} &:= \sup_{z\in\mathcal{C}} |D^3 f_{e_0}(z)| \ , \\
Q_{ezz} &:= \sup_{z\in\mathcal{C},e\in\Lambda,|e-e_0|<2\kappa_e\varepsilon_0} |D^2 D_e f_e(z)| \ , \\
Q_{ze} &:= \sup_{z\in\mathcal{C},e\in\Lambda,|e-e_0|<2\kappa_e\varepsilon_0} |D_e Df_e(z)| \ , \\
Q_{ee} &:= \sup_{z\in\mathcal{C},e\in\Lambda,|e-e_0|<2\kappa_e\varepsilon_0} |D_e^2 f_e(z)| \ , \\
Q_{zze} &:= \sup_{z\in\mathcal{C},e\in\Lambda,|e-e_0|<2\kappa_e\varepsilon_0} |D_e D^2 f_e(z)| \ , \\
Q_{eez} &:= \sup_{z\in\mathcal{C},e\in\Lambda,|e-e_0|<2\kappa_e\varepsilon_0} |DD_e^2 f_e(z)| \ , \\
Q_{eee} &:= \sup_{z\in\mathcal{C},e\in\Lambda,|e-e_0|<2\kappa_e\varepsilon_0} |D_e^3 f_e(z)| \ , \\
Q_{E0} &:= \frac{1}{2}\max\left\{ \|D^2 E_0\|_{\rho_0-\delta_0}, \|DD_e E_0\|_{\rho_0-\delta_0}, \|D_e^2 E_0\|_{\rho_0-\delta_0} \right\} \ .
\end{aligned}
\tag{25}
$$

Assume that ε_0 is such that the following smallness conditions are satisfied for real constants $C_{\eta 0}$, $C_{\mathcal{E}0}$, C_{d0}, $C_{\sigma 0}$, C_σ, C_{W0}, C_W and $C_{\mathcal{R}}$ (see Appendix A):

$$C_{\eta 0}\,\nu^{-1}\delta_0^{-\tau}\varepsilon_0 < \zeta \ , \tag{26}$$

$$2^{3\tau+4}\,C_{\mathcal{E}0}\,\nu^{-2}\,\delta_0^{-2\tau}\varepsilon_0 \le 1 \ , \tag{27}$$

$$4C_{d0}\nu^{-1}\delta_0^{-\tau}\varepsilon_0 < \zeta \ , \tag{28}$$

$$4C_{\sigma 0}\varepsilon_0 < \zeta \ , \tag{29}$$

$$\|N_0\|_{\rho_0}\,(2\|DK_0\|_{\rho_0}+D_K)\,D_K < 1 \ , \tag{30}$$

$$4Q_{ze0}C_{\sigma 0}\varepsilon_0 < Q_z \ , \tag{31}$$

$$4Q_{ee}C_{\sigma 0}\varepsilon_0 < Q_e \ , \tag{32}$$

$$C_\sigma\ D_K \le C_{\sigma 0} \ , \tag{33}$$

$$D_K(C_{W0}+\|M_0\|_{\rho_0}C_W+C_W D_K) \le C_{d0} \ , \tag{34}$$

$$D_K\left(C_W\ \nu\delta_0^{-1+\tau}+C_{\mathcal{R}}\right) \le C_{\mathcal{E}0} \ , \tag{35}$$

where D_K is given by

$$D_K := 4C_{d0}\ \nu^{-1}\delta_0^{-\tau-1}\ \varepsilon_0 \ . \tag{36}$$

Then, there exists an exact solution (K_*, e_*) of (21) satisfying

$$f_{e_*}\circ K_* - K_*\circ T_\omega = 0 \ .$$

The following inequalities show that the quantities (K_*, e_*) are close to (K_0, e_0):

$$
\begin{aligned}
\|K_*-K_0\|_{\rho_0-\delta_0} &\le 4C_{d0}\nu^{-1}\delta_0^{-\tau}\|E_0\|_{\rho_0} \ , \\
|e_*-e_0| &\le 4C_{\sigma 0}\|E_0\|_{\rho_0} \ ,
\end{aligned}
\tag{37}
$$

where C_{d0} and $C_{\sigma 0}$ are given explicitly in Appendix A.

For simplicity of exposition, we report the explicit expressions of the constants entering Theorem 4.6 in Appendix A. They are obtained making a constructive version of the KAM proof given in [10]. We refer to [15] for the proof of Theorem 4.6.

4.5. A sketch of the proof of Theorem 4.6

We present a sketch of the proof of Theorem 4.6 that we split into five main steps, all of them giving explicit estimates of the quantities involved. Although we do not enter into the details of the proof, which is quite long and technical

(see [15]), we provide an overview of the proof which motivates the assumptions H1–H5 as well as the smallness conditions (26)-(35).

4.5.1. Step 1: the approximate solution

We denote by (K, e) an embedding function and a drift term satisfying approximately the invariance equation with an error term E:

$$f_e \circ K(\theta) - K(\theta + \omega) = E(\theta) \, . \tag{38}$$

All one-dimensional tori are Lagrangian invariant tori, namely they satisfy $K^*\Omega = 0$, which in coordinates is given by

$$DK^T(\theta)\, J \circ K(\theta)\, DK(\theta) = 0 \, .$$

This expression implies that the tangent space can be decomposed as the sum of the range of $DK(\theta)$ and the range of $V(\theta)$, where V is given by

$$V(\theta) = J^{-1} \circ K(\theta)\, DK(\theta) N(\theta)$$

with $N(\theta) = (DK(\theta)^\top DK(\theta))^{-1}$.

Next, we define the quantity M as a juxtaposition of DK and V, i.e.,

$$M(\theta) = [DK(\theta) \mid V(\theta)] \, . \tag{39}$$

Then, it can be shown that, up to a remainder R, the action of the derivative of the map over M is just a shift of M multiplied by a matrix. Precisely, one can prove that [15]:

$$Df_e \circ K(\theta)\, M(\theta) = M(\theta + \omega) \begin{pmatrix} \mathrm{Id} & S(\theta) \\ 0 & \lambda \mathrm{Id} \end{pmatrix} + R(\theta) \, . \tag{40}$$

This result will be used in Step 2 to reduce (38) to a constant coefficient equation, that will be solved under assumptions H1 and H3.

4.5.2. Step 2: a new approximation

Starting from the initial approximation (K, e), we introduce a new approximation (K', e') defined adding to (K, e) some corrections (W, σ) as $K' = K + MW$ and $e' = e + \sigma$. We denote by E' the error function associated to (K', e'), satisfying the equation:

$$f_{e'} \circ K'(\theta) - K'(\theta + \omega) = E'(\theta) \, . \tag{41}$$

Next, we proceed to expand (41) in Taylor series, which gives:

$$\begin{aligned} & f_e \circ K(\theta) + Df_e \circ K(\theta)\, M(\theta) W(\theta) + D_e f_e \circ K(\theta)\sigma \\ & -K(\theta + \omega) - M(\theta + \omega)\, W(\theta + \omega) + h.o.t. = E'(\theta). \end{aligned}$$

Using (38), we can guarantee that E' is quadratically smaller provided that the following relation is satisfied:

$$Df_e \circ K(\theta)\, M(\theta) W(\theta) - M(\theta + \omega)\, W(\theta + \omega) + D_e f_e \circ K(\theta)\sigma = -E(\theta) \, . \tag{42}$$

We remark that condition (26) provides an estimate of the error E' associated to (K', e').

Using (42) and (40), we obtain that

$$Df_e \circ K(\theta)\, M(\theta) = M(\theta + \omega) \begin{pmatrix} \mathrm{Id} & S(\theta) \\ 0 & \lambda \mathrm{Id} \end{pmatrix} + R(\theta) \, ,$$

which provides the following equations for W and e:

$$M(\theta + \omega) \begin{pmatrix} \mathrm{Id} & S(\theta) \\ 0 & \lambda \mathrm{Id} \end{pmatrix} W(\theta) - M(\theta + \omega)\, W(\theta + \omega) = -E(\theta) - D_e f_e \circ K(\theta)\sigma \, . \tag{43}$$

Next, we multiply by $M(\theta + \omega)^{-1}$ and write (43) for the components W_1, W_2, $\tilde{E}_1$, $\tilde{E}_2$, $\tilde{A}_1$, $\tilde{A}_2$, of W, $\tilde{E}$, and $\tilde{A}$ as

$$\begin{pmatrix} \mathrm{Id} & S(\theta) \\ 0 & \lambda \mathrm{Id} \end{pmatrix} \begin{pmatrix} W_1(\theta) \\ W_2(\theta) \end{pmatrix} - \begin{pmatrix} W_1(\theta + \omega) \\ W_2(\theta + \omega) \end{pmatrix} = \begin{pmatrix} -\tilde{E}_1(\theta) - \tilde{A}_1(\theta)\sigma \\ -\tilde{E}_2(\theta) - \tilde{A}_2(\theta)\sigma \end{pmatrix} \, , \tag{44}$$

where we define

$$\begin{aligned} \tilde{E}_j(\theta) &= -(M(\theta + \omega)^{-1} E)_j \\ \tilde{A}_j(\theta) &= (M(\theta + \omega)^{-1} D_e f_e \circ K)_j \, , \end{aligned}$$

for $j = 1, 2$. We now make explicit (44) for the components W_1, W_2 and σ, so to obtain the following cohomological equations:

$$\begin{aligned} W_1(\theta) - W_1(\theta + \omega) &= -\widetilde{E}_1(\theta) - S(\theta) W_2(\theta) - \widetilde{A}_1(\theta)\sigma \\ \lambda W_2(\theta) - W_2(\theta + \omega) &= -\widetilde{E}_2(\theta) - \widetilde{A}_2(\theta)\sigma \, . \end{aligned} \tag{45}$$

4.5.3. Step 3: Determination of the new approximate solution

The solution of equations (45) allow us to determine the unknowns W_1, W_2 and σ that give the corrections to determine the new approximate solution.

To solve the first equation of (45), we use assumption H1 on the Diophantine property of the frequency and assumption H3, expressing the non-degeneracy that allows us to solve the linear system (46) below. The second equation of (45) can instead be solved by an elementary contraction mapping argument for any $|\lambda| \neq 1$ and for all real frequencies.

Let us write W_2 as $W_2 = \langle W_2 \rangle + B^0 + \tilde{B}^0 \sigma$. Taking the average of both equations (45), we obtain the equations

$$\begin{pmatrix} \langle S \rangle & \langle SB^0 \rangle + \langle \widetilde{A}_1 \rangle \\ (\lambda - 1)\mathrm{Id} & \langle \widetilde{A}_2 \rangle \end{pmatrix} \begin{pmatrix} \langle W_2 \rangle \\ \sigma \end{pmatrix} = \begin{pmatrix} -\langle S\tilde{B}^0 \rangle - \langle \widetilde{E}_1 \rangle \\ -\langle \widetilde{E}_2 \rangle \end{pmatrix} , \tag{46}$$

which can be solved to give $\langle W_2 \rangle$ and σ under the non-degeneracy condition H3.

Once the solution of (46) is obtained, we proceed to solve the second of (45) to determine W_2; such equation can be solved for any $|\lambda| \neq 1$ by a contraction mapping argument.

Then, we proceed to solve the first equation of (45) for W_1: since it involves small divisors, we can solve the equation under the Diophantine assumption H1. The quantities $\|W_1\|_{\rho-\delta}$ and $\|W_2\|_{\rho-\delta}$ can be bounded by $\|E\|_\rho$ by using Cauchy estimates for the cohomological equations (45).

The error E' associated to the new solution can be bounded on a domain of size $\rho - \delta$ by the square of the error E on the domain of size ρ as

$$\|E'\|_{\rho-\delta} \leq C_E \delta^{-2\tau} \|E\|_\rho^2 , \qquad C_E > 0 ,$$

showing that the new error of the procedure is quadratic in the original error. Assumption H4 is needed to obtain such a bound.

4.5.4. Step 4: iteration and convergence

We proceed to iterate the procedure presented in Step 3 to obtain a sequence of new solutions, say $\{K_j, e_j\}$, and their associated invariance equation error, say E_j. We prove that the errors tends to zero (in suitable norms) as $j \to \infty$ and thus the solution sequence converges to the true solution. The proof consists in implementing an abstract implicit function theorem, alternating the iteration with carefully chosen smoothing operators for analytic functions. The smoothing is obtained by rescaling domains where the functions are defined at each step. In particular, we can define as ρ_j the size of the analyticity domain associated to the solution $\{K_j, e_j\}$ by introducing a shrinking parameter δ_j and setting

$$\rho_0 = \rho , \qquad \delta_j = \frac{\rho_0}{2^{j+2}} , \qquad \rho_{j+1} = \rho_j - \delta_j , \qquad j \geq 0 .$$

Then, we can show that for $a, b > 0$ and $C_E' > 0$, we have

$$\|E_{j+1}\|_{\rho_{j+1}} \leq C_E' \, \nu^a \delta_j^b \, \|E_j\|_{\rho_j}^2 .$$

If the quantity $\varepsilon_0 \equiv \|E_0\|_{\rho_0}$ is sufficiently small, then we conclude that

$$\|K_j - K_0\|_{\rho_j} \leq C_K \varepsilon_0 , \qquad |e_j - e_0| \leq C_\mu \varepsilon_0 \tag{47}$$

for some constants $C_K, C_\mu > 0$. The inequalities (26)-(35) of Theorem 4.6 allow to obtain (47) as well as to ensure that the procedure can be iterated and that it converges to the true solution.

4.5.5. Step 5: local uniqueness

Under smallness conditions, one can prove that, if there exist two solutions (K_a, e_a), (K_b, e_b), then there exists $\psi \in \mathbb{R}$ such that

$$K_b(\theta) = K_a(\theta + \psi) \qquad \text{and} \qquad e_a = e_b .$$

4.6. The algorithm and the initial invariant curve

Theorem 4.6 provides an explicit algorithm working as follows: for a fixed frequency ω and from an approximate solution (K_0, e_0) satisfying the invariance equation with error term E_0, one can construct a new approximation (K_1, e_1) satisfying the invariance equation with a new error term E_1 which is quadratically smaller than E_0, just taking derivatives and performing algebraic operations. The new approximation is obtained by solving suitable cohomological equations, under the non-degeneracy condition H3. The algorithm is presented in detail in [14] for the spin–orbit problem and it is recalled in Appendix B.

In the following, we will consider two frequencies defined as

$$\omega_1 := \gamma_g^+ \tag{48}$$

and

$$\omega_2 := 1 + \frac{1}{2 + \gamma_g^-} , \tag{49}$$

where $\gamma_g^{\pm} := \frac{\sqrt{5}\pm 1}{2}$. Both frequencies are Diophantine, in the sense of Definition 4.2, with constant $\nu = (\frac{3-\sqrt{5}}{2})^{-1}$ and exponent $\tau = 1$.

The application of Theorem 4.6 consists in the steps given below.

(i) We fix the Diophantine frequency as one of the choices in (48) or (49).
(ii) We provide the initial values K_0 and e_0, selecting the eccentricity and the initial condition as follows. First, we select the eccentricity by choosing the value that corresponds to the fixed frequency. This is achieved by integrating Eq. (2) with an initial guess of e_0 and initial conditions $x(0) = 0$ and we fix $y(0) = \bar{N}(e_0)/\bar{L}(e_0)$, which is the value that we obtain when the dissipation disappears in the averaged model (3). After a transient time t (so that the system evolves on the attractor), we compute the frequency over N_{it} additional iterations as $\omega = \frac{1}{N_{it}} \sum_{j=1}^{N_{it}} y(t + 2\pi j)$. Once the approximated initial eccentricity for the desired frequency has been obtained, we iterate the Poincaré map (after another suitable transient) and we obtain the initial approximation of the invariant curve by fitting the discrete points.
(iii) We iterate Algorithm B.1 to obtain a more accurate approximation (K_a, e_a) satisfying the invariance equation with an error whose norm is sufficiently small.
(iv) We compute the norms of the quantities appearing in Theorem 4.6 and detailed in Appendix D for ω_1 and Appendix E for ω_2.
(v) We check the conditions (26)-(35) in Theorem 4.6. If they are satisfied, we conclude the procedure, otherwise we change some of the parameters (e.g., ρ and δ) and we try to optimize the final result.

Further details of the steps (ii) and (iii) can be found in [14], which contains also the computation of the variational equations with respect to the initial conditions and the parameter e in (2). The rotation number in (ii) can be computed more efficiently (with smaller N_{it}) by [27]. The variational equations are needed in step 7 of the Algorithm B.1 in Appendix B as well as for some of the quantities in (iv).

4.7. Continuation method

Algorithm B.1 can be used as a corrector for a continuation method of the invariant torus and its drift. In the spin–orbit problem, we use the eccentricity e as the adjustable parameter required by the quasi-Newton method and the perturbative parameter ε in (2) as the continuation parameter.

The continuation consists in increasing ε by a stepsize, say ε_h, and run the Algorithm B.1 again with a given Newton's tolerance $\tilde{\epsilon}$. Thus at each continuation step, it succeed, we obtain a new embedding of the torus and a new corrected eccentricity.

If $\varepsilon + \varepsilon_h$ converges, we increase ε_h for the next continuation step. Otherwise, we do not accept $\varepsilon + \varepsilon_h$ as a solution, we decrease ε_h, and we use Algorithm B.1 with the new value of $\varepsilon + \varepsilon_h$. In both cases we perform a Lagrange interpolation of the previous two or three steps in order to provide a better initial guess of K and e for the next iteration.

In all the above process, a refinement of the grid in the coordinate θ may be required. In our implementation, we consider necessary to increase the number of Fourier coefficients when some of the following two cases arise.

The first one is when the accuracy tests, detailed in Section 5.3 of [14], fail. In short, the accuracy tests are aimed to control different sources of error, precisely:

(1) the error of the invariance equation on a table of values;
(2) the error in the numerical integration, for which we introduce absolute and relative tolerances;
(3) the error in the grid over the coordinate θ, which is controlled by checking the last coefficients of the truncated Fourier series as well as the Sobolev norm of the tail;
(4) the interpolation error, which is controlled by providing an estimate of it and by changing the size of the grid, when the error becomes too large.

The second situation is when the continuation step fails consecutively two times which may require to decrease the stepsize ε_h, especially when we are getting close to the breakdown. Thus, the continuation procedure will stop when the maximum number of remeshing is reached, in our case 2^{14} Fourier modes.

Fig. 1 displays the results of the KAM torus (black curve) after a continuation starting at $\varepsilon = 10^{-4}$ and a fixed dissipation $\eta = 10^{-3}$. The computation has been done with a multi-precision arithmetic with 170 bits, i.e. around 50 digits of accuracy, a Newton's tolerance of $\tilde{\epsilon} = 10^{-35}$, and a parallelization of the integration of the Poincaré map as detailed in Section 5.5 of [14].

We emphasize that we checked the final result by changing the number of digits of accuracy; in other words, keeping the same Newton's tolerance $\tilde{\epsilon}$ and the same integration's tolerance, we have performed the last continuation step, checking that it is satisfied with 50, 55, and 60 digits of accuracy.

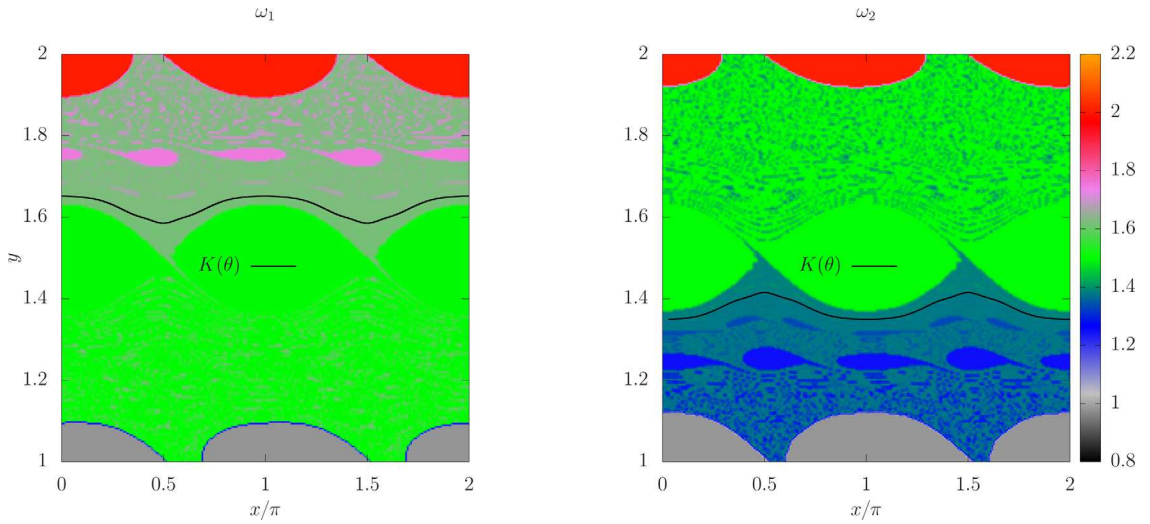

Fig. 1. Basins of rotation number given by color-scale for the parameters in (51) (left) and (50) (right) joined with the of Algorithm B.1 that show the invariant attractor (in black) after a continuation of ε starting with $\varepsilon = 10^{-4}$ and $e = 0.3150628$ (left) and $e = 0.2502068$ (right).

The values of the Fourier modes n_θ, the dissipation η, the eccentricity e, and the perturbing parameter ε are reported below for the Diophantine frequencies ω_1 in (48) and ω_2 in (49).

For ω_1, the last successful Newton continuation step was reached in less than 3 min using 32 CPUs with final values:

$$\begin{aligned} n_\theta &= 16384\ , \\ \eta &= 10^{-3}\ , \\ e &= 0.31675286891174832107186084513865661761571784973618\ , \\ \varepsilon &= 0.01163296364187711636771611264294853055967553138229 7\ . \end{aligned} \tag{50}$$

For ω_2 we got the last successful torus in less than 5 min using 35 CPUs and with values:

$$\begin{aligned} n_\theta &= 4096\ , \\ \eta &= 10^{-3}\ , \\ e &= 0.24824740823563165902227100091869770425731996450084\ , \\ \varepsilon &= 0.01269763002441588303212383001366761350900995082616 8\ . \end{aligned} \tag{51}$$

Fig. 1 provides also the basins of the rotation numbers, namely the frequency given through a color scale for different initial conditions (x_0, y_0). In particular, we take a grid of 500×500 initial conditions within the window $[0, 2\pi) \times [1, 2]$ and we compute the frequency as described in step (ii) of Section 4.6. We remark that the computation of the frequency has been optimized using the method described in [27] which is implemented and detailed for the spin–orbit case in the companion paper [28].

5. Estimates on the Q quantities of the KAM Theorem 4.6

The main difference in the explicit derivation of the KAM estimates presented in [15] between the standard map and the spin–orbit problem is the computation of the Q constants defined in (25) of Theorem 4.6. Almost all of them are zero for the standard map, while for the spin–orbit problem we need to compute them as detailed in Sections 5.1 and 5.2 below.

It is also important to describe carefully the boundary of the domain $\mathcal{C}$ and, in particular, the value ζ in H4 which is needed for the inequalities (26)–(35).

5.1. The computation of Q_{E0}

We need to give a bound of the quantity

$$Q_{E_0} := \frac{1}{2} \max\left\{ \|D^2 E_0\|_{\rho_0-\delta_0}, \|D_e D E_0\|_{\rho_0-\delta_0}, \|D_e^2 E_0\|_{\rho_0-\delta_0} \right\}\ , \tag{52}$$

where E_0 is defined in terms of the numerical approximated solution (K_0, e_0) of Theorem 4.6. In the case of the spin–orbit problem, E_0 is given by

$$\mathcal{E}(\theta) := (\Psi_{e_0}^{-1} \circ G_{e_0})^1(\Psi_{e_0} \circ K_0(\theta)) - K_0^1(\theta + \omega) ,$$
$$E_0^1(\theta) := \mathcal{E}(\theta) - \lfloor \mathcal{E}(\theta) + 0.5 \rfloor , \tag{53}$$
$$E_0^2(\theta) := (\Psi_{e_0}^{-1} \circ G_{e_0})^2(\Psi_{e_0} \circ K_0(\theta)) - K_0^2(\theta + \omega) , \tag{54}$$

where $\lfloor \cdot \rfloor$ denotes the floor function, e_0 is the eccentricity value, $G_{e_0} = \Psi_{e_0} \circ P_{e_0} \circ \Psi_{e_0}^{-1}$ with P_{e_0} being the 2π-time flow of (2) and Ψ_{e_0} given in (6). The superscripts ^{1} and ^{2} mean the components of the vectors in $\mathbb{R}^2$. Note that the floor function in (53) is needed since $x(t)$ in (2) is given modulus 2π, that due to Ψ_{e_0}, in fact, it is modulus 1. Therefore E_0^1 gives values in $[-1/2, 1/2]$.

To compute $D^2 E_0$ we can either differentiate the Fourier series with respect to θ or to use jet transport, which, roughly speaking, means to overload the numerical integrator with a multivariate polynomial manipulator. We are going to use the jet transport because we also need to get the variation with respect to the eccentricity, i.e., $D_e D E_0$ and $D_e E_0$. In order to get the quantities automatically, we use jets[2] of 2 symbols, say (s_1, s_2), and up to degree 2, see Appendix F. Indeed, for each θ in a mesh of $\mathbb{T}$, we compute the flow given by

$$\Psi_{e_0+s_2}^{-1} \circ G_{e_0+s_2} \circ \Psi_{e_0+s_2}(K_0(\theta + s_1)) , \tag{55}$$

where

$$K_0(\theta + s_1) = K_0(\theta) + \partial_\theta K_0(\theta) s_1 + \tfrac{1}{2} \partial_\theta^2 K_0(\theta) s_1^2 .$$

Remark 5.1. Jet transport will provide the normalized derivative of (55), so the 1/2 in (52) is automatically included in the coefficients of degree 2 of (55). Notice that here, we can use the ad hoc polynomial manipulator described in Appendix F.

Remark 5.2. The term $\lfloor \cdot + 0.5 \rfloor$ in (53) refers to the `round` function, namely the function that returns the nearest integer, but round halfway cases away from zero, regardless of the current rounding direction, and instead of the nearest integer in the `rint` function.

Note that `round` has zero derivative except in $(\frac{1}{2}\mathbb{Z}) \setminus \{0\}$, where the derivative is not well-defined. However, we will consider (numerically) derivative zero also in these discontinuity points.

Remark 5.3. About the 2nd derivatives for the term $K_0(\theta + \omega)$, the ones with respect to e are zero and the computation of $\partial_\theta^2 K_0(\theta + \omega)$ is straightforward in the Fourier representation.

Remark 5.4. The computation of (55) is fully parallelizable for each of the different values of θ, which gives us a clear speed-up in the performance. Specially when the quantity is computed near to the breakdown parameter value that, generically, requires more Fourier modes.

5.2. The computation of the complex Q's in Theorem 4.6

The quantities in the hypothesis H5 of Theorem 4.6 require to perform the integration of complex numbers, since the initial conditions are in the complex domain $\mathcal{C}$, in fact, in its boundary. The complexification of the spin–orbit model leads to the *complex spin–orbit* problem, see Section 5.2.1, which is given as a real 4-dimensional ODE system. This system describes the evolution in time of the real and imaginary parts of each of the variables in (2).

To address some of the freedoms in Theorem 4.6, we devote our attention in Section 5.2.2 to provide a definition of a possible domain $\mathcal{C}$ such that we can fulfill the hypothesis H4. The strategy will be to move this original freedom on $\mathcal{C}$ to two new parameters, ξ and α, which are going to be easier to handle.

Finally, we detail in Section 5.3 the different steps to approximate the Q quantities of H5.

5.2.1. Complex spin–orbit problem

The Q quantities in (25) are considered over the complex domain $\mathcal{C}$ of Theorem 4.6. This implies the need of the complexification of the spin–orbit problem (2), which leads to a new system called the *complex spin–orbit problem* given

[2] We follow the convention that a jet is encoded by the Taylor's coefficients at 0.

by the real ODE system

$$\begin{aligned}
&\frac{d}{dt}x_{\mathtt{R}}(t) = y_{\mathtt{R}}(t)\,,\\
&\frac{d}{dt}x_{\mathtt{I}}(t) = y_{\mathtt{I}}(t)\,,\\
&\frac{d}{dt}y_{\mathtt{R}}(t) = -\varepsilon\Big(\frac{a}{r(t)}\Big)^3 \sin\big(2x_{\mathtt{R}}(t)-2f(t)\big)\cosh(2x_{\mathtt{I}}(t)) - \eta\Big(\frac{a}{r(t)}\Big)^5 \big(y_{\mathtt{R}}(t)-\frac{d}{dt}f(t)\big)\,,\\
&\frac{d}{dt}y_{\mathtt{I}}(t) = -\varepsilon\Big(\frac{a}{r(t)}\Big)^3 \cos\big(2x_{\mathtt{R}}(t)-2f(t)\big)\sinh(2x_{\mathtt{I}}(t)) - \eta\Big(\frac{a}{r(t)}\Big)^5 y_{\mathtt{I}}(t)\,,
\end{aligned} \tag{56}$$

where (56) has been deduced by taking the complex numbers $x = x_{\mathtt{R}} + \mathtt{i}y_{\mathtt{I}}$ and $y = x_{\mathtt{R}} + \mathtt{i}y_{\mathtt{I}}$ in (2). To obtain the above equations, we use the relation

$$\sin(\alpha_{\mathtt{R}} + \mathtt{i}\alpha_{\mathtt{I}}) = \sin\alpha_{\mathtt{R}}\cosh\alpha_{\mathtt{I}} + \mathtt{i}\cos\alpha_{\mathtt{R}}\sinh\alpha_{\mathtt{I}}\,.$$

Similarly to the real spin–orbit problem, see [14], we consider the temporal change of coordinates $t = u - e\sin u$ to make u the independent variable, i.e.,

$$\begin{aligned}
&x_{\mathtt{R}}(u-e\sin u) =: \beta_{\mathtt{R}}(u)\,, \quad y_{\mathtt{R}}(u-e\sin u) =: \gamma_{\mathtt{R}}(u)/(1-e\cos u)\,,\\
&x_{\mathtt{I}}(u-e\sin u) =: \beta_{\mathtt{I}}(u)\,, \quad y_{\mathtt{I}}(u-e\sin u) =: \gamma_{\mathtt{I}}(u)/(1-e\cos u)\,.
\end{aligned} \tag{57}$$

Thus, if $\widehat{G}_e$ is the 2π-time flow of the complex spin–orbit problem with the coordinates $(\beta_{\mathtt{R}}, \beta_{\mathtt{I}}, \gamma_{\mathtt{R}}, \gamma_{\mathtt{I}})$, then we can recover the normalized 2π-time flow $\widehat{P}_e$ of (56) by the conjugacy given by

$$\widehat{\Psi}_e := 2\pi \begin{pmatrix} 1 & 0 & 0 & 0\\ 0 & 1 & 0 & 0\\ 0 & 0 & 1-e & 0\\ 0 & 0 & 0 & 1-e \end{pmatrix}\,.$$

Explicitly, we obtain:

$$\widehat{P}_e := \widehat{\Psi}_e^{-1} \circ \widehat{G}_e \circ \widehat{\Psi}_e\,. \tag{58}$$

Therefore to get the different high variational flows involved in the Q quantities of H5, we can use the jet transport technique, see [14], with jets of 5 symbols and up to order 3.

5.2.2. Definition of the boundary of the complex domain $\mathcal{C}$

The Q quantities of the hypothesis H5 depend on the boundary $\partial\mathcal{C}$, because the ODE (2) as well as (56) are analytic. The only restriction on this set $\partial\mathcal{C}$ is given in H4 which relates the distance of the set

$$K_0(\mathbb{T}_{\rho_0}) := \left\{ \begin{pmatrix} \theta + \mathtt{i}\sigma \\ 0 \end{pmatrix} + \overline{K}_0(\theta + \mathtt{i}\sigma) : \theta \in \mathbb{T} \text{ and } |\sigma| \le \rho_0 \right\}$$

with $\overline{K}_0$ denoting the periodic part of the mapping K_0 which is continuously extended to the boundary of the set $\mathbb{T}_{\rho_0}$ defined in (12).

Recall that the distance between sets is defined by

$$\mathrm{dist}(K_0(\mathbb{T}_{\rho_0}), \partial\mathcal{C}) := \inf\{d(x,y) : x \in K_0(\mathbb{T}_{\rho_0}) \text{ and } y \in \partial\mathcal{C}\}\,.$$

Hence, we consider $\mathcal{C}$ given in terms of a real region Ξ in the plane and a real value $\alpha > 0$, as

$$\mathcal{C} := \{(z_1, z_2) \in \mathbb{C}/\mathbb{Z} \times \mathbb{C} : (z_1, z_2) \in \Xi,\ |z_1| \le \alpha,\ |z_2| \le \alpha\}\,.$$

The region Ξ is bounded and we assume to be of the form

$$\Xi := \{(\theta, \sigma) \in \mathbb{T} \times \mathbb{R} : \psi_-(\theta) \le \sigma \le \psi_+(\theta)\}$$

for some real curves ψ_- and ψ_+ such that

$$\psi_- \circ K_0^1(\theta) \le K_0^2(\theta) \le \psi_+ \circ K_0^1(\theta) \quad \text{for all } \theta \in \mathbb{T}\,.$$

For instance, fixed $\xi > 0$, one can try to find $\psi_\pm$ solving

$$\psi_\pm \circ K_0^1(\theta) = K_0^2(\theta) \pm \xi \quad \text{for all } \theta \in \mathbb{T}\,.$$

Then, $K_0(\theta) \in \Xi$ for all θ in $\mathbb{T}$. Heuristically, $K_0^1(\theta) = \theta + \overline{K}_0^1(\theta) \approx \theta$, if $\overline{K}_0^1$ is small and the composition by K_0^1 may be neglected. In fact, if we allow constant values for $\psi_\pm$, we can just consider

$$\psi_- := \min_{\theta\in\mathbb{T}} K_0^2(\theta) - \xi\,, \qquad \psi_+ := \max_{\theta\in\mathbb{T}} K_0^2(\theta) + \xi \tag{59}$$

with a suitable value of ξ.

Let us assume that (depending on α and $\psi_\pm$)

$$\partial\mathcal{C} := A_\pm \cup B_\pm \cup C_\pm \,, \tag{60}$$

where

$$\begin{aligned}
A_\pm &:= \{(\theta + \mathtt{i}x, \psi_\pm(\theta) + \mathtt{i}y) : \theta \in \mathbb{T},\ |x| \le \alpha,\ |y| \le \alpha\} \,,\\
B_\pm &:= \{(\theta \pm \mathtt{i}\alpha, v + \mathtt{i}w) : \theta \in \mathbb{T},\ \psi_-(\theta) \le v \le \psi_+(\theta),\ |w| \le \alpha\} \,,\\
C_\pm &:= \{(\theta + \mathtt{i}\sigma, v \pm \mathtt{i}\alpha) : \theta \in \mathbb{T},\ \psi_-(\theta) \le v \le \psi_+(\theta),\ |\sigma| \le \alpha\} \,.
\end{aligned}$$

We have different cases to get a lower bound on $\mathrm{dist}(K_0(\mathbb{T}_{\rho_0}), \partial\mathcal{C})$. Let us consider generic points

$$\begin{aligned}
x &= \left(\theta + \mathtt{i}\sigma + \overline{K}_0^1(\theta + \mathtt{i}\sigma)\,, \overline{K}_0^2(\theta + \mathtt{i}\sigma)\right) \in K_0(\mathbb{T}_{\rho_0}) \,,\\
a_1^\pm &= (\theta_1 + \mathtt{i}x_1, \psi_\pm(\theta_1) + \mathtt{i}y_1) \in A_\pm \,,\\
b_1^\pm &= (\theta_1 \pm \mathtt{i}\alpha, v_1 + \mathtt{i}w_1) \in B_\pm \,,\\
c_1^\pm &= (\theta_1 + \mathtt{i}\sigma_1, v_1 \pm \mathtt{i}\alpha) \in C_\pm \,.
\end{aligned}$$

If we use $\psi_\pm$ constants, as those defined in (59), then we need to compute the Υ_i quantities given by

$$\begin{aligned}
|x - a_1^+| &\ge \inf_{\theta+\mathtt{i}\sigma\in\mathbb{T}_{\rho_0}} |K_0^2(\theta + \mathtt{i}\sigma) - \psi_+| =: \Upsilon_1 \,,\\
|x - a_1^-| &\ge \inf_{\theta+\mathtt{i}\sigma\in\mathbb{T}_{\rho_0}} |K_0^2(\theta + \mathtt{i}\sigma) - \psi_-| =: \Upsilon_2 \,,\\
|x - b_1^+| &\ge \inf_{\theta+\mathtt{i}\sigma\in\mathbb{T}_{\rho_0}} |K_0^1(\theta + \mathtt{i}\sigma) - \alpha| =: \Upsilon_3 \,,\\
|x - b_1^-| &\ge \inf_{\theta+\mathtt{i}\sigma\in\mathbb{T}_{\rho_0}} |K_0^1(\theta + \mathtt{i}\sigma) + \alpha| =: \Upsilon_4 \,,\\
|x - c_1^+| &\ge \inf_{\theta+\mathtt{i}\sigma\in\mathbb{T}_{\rho_0}} |K_0^2(\theta + \mathtt{i}\sigma) - \alpha| =: \Upsilon_5 \,,\\
|x - c_1^-| &\ge \inf_{\theta+\mathtt{i}\sigma\in\mathbb{T}_{\rho_0}} |K_0^2(\theta + \mathtt{i}\sigma) + \alpha| =: \Upsilon_6 \,.
\end{aligned} \tag{61}$$

Thus, if we take $\Upsilon := \min\{\Upsilon_1, \Upsilon_2, \Upsilon_3, \Upsilon_4, \Upsilon_5, \Upsilon_6\}$, then

$$\mathrm{dist}(K_0(\mathbb{T}_{\rho_0}), \partial\mathcal{C}) \ge \Upsilon \,. \tag{62}$$

Therefore, we can choose ζ so that $\Upsilon \ge \zeta > 0$. Finally, we can set $\Lambda := (e_0 - \varphi, e_0 + \varphi)$ with $\varphi \ge \max\{\zeta, 2\kappa_e\varepsilon_0\}$ and κ_e given in H5.

Note that the computation of Υ_i in (61) does not need to be rigorous, because we can take ζ further smaller than the approximated Υ.

A second remark in the computation of Υ_i is that we can use the complex version of the FFT to make the computation faster. Indeed, using Appendix C, we complexify the real representation of the Fourier coefficients of K_0 and then use the FFT to get the corresponding table of values in an equispaced complex plane $\mathbb{T}_{\rho_0}$. This process makes the computation of an approximated Υ efficient, easily running in a today's laptop without a strong need of concurrency.

5.3. Steps to approximate the Q quantities

Once we obtain the initial numerical approximate solution (K_0, e_0) of the invariance Eq. (21) via the Newton Algorithm B.1, we choose $0 < \rho_0 < 1$ to compute the different quantities involved in the KAM estimates of Theorem 4.6. That means to compute the quantities of H5 and the constants in Appendix A. The constants only depend on norms of functions from the Algorithm B.1 like $\|DK_0\|_{\rho_0}$, $\|DK_0^{-1}\|_{\rho_0}$, $\|N\|_{\rho_0}$, $\|S\|_{\rho_0}$, etc. The Q quantities require more effort and we will use the procedure described in Section 5.2.

The first Q quantity Q_{E_0} in Section 5.1 requires to choose $0 < \delta_0 < \rho_0$. For the other Q quantities in Section 5.2 we need first to choose ξ to get $\psi_\pm$ from (59) and α for (60). Then we compute the Υ such that (62) is satisfied. Finally, we can choose ζ which is the last crucial value that fixes all the other quantities to check the inequalities (26)–(35).

We note that the complex quantities of Q, which in fact are the hardest ones, do not need to be extremely rigorous because especially for those involving high order variational flows, they are always affected by the multiplication of small values, like the ε_0, as one can realize looking at (26)–(35) and Appendix A. Therefore, our approach will just consider the quantities in a mesh of the six sets in (60), rather than a rigorous enclosure. In fact, we also compensate the correctness of our numbers using multiprecision, that was already needed to reach parameter values close to the numerical break-down.

6. KAM estimates for the spin–orbit problem

The application of Theorem 4.6 requires to check the conditions (26)–(35) that depend on the choice of some parameters. We did not found a general procedure to select ρ_0, δ_0, ξ, α and ζ, so that we can ensure a priori that the inequalities will be fulfilled. Nevertheless, we provide the values of these numbers for the cases ω_1 and ω_2 with respective spin–orbit parameters given in (50) and (51).

In the two cases ω_1 in (50) and ω_2 in (51), by trial and error we have made the following choice:

$$\begin{aligned} \rho_0 &= 7.629394531250000 \cdot 10^{-6} = 2^{-17} \,, \\ \delta_0 &= 9.536743164062500 \cdot 10^{-7} = 2^{-20} \,, \\ \xi &= 0.0054 \,, \\ \alpha &= 0.000016 \,, \\ \zeta &= 9.313225746154785625\,00 \cdot 10^{-10} = 2^{-30} \,. \end{aligned} \tag{63}$$

Note that ρ_0, δ_0, and ζ are just a power of 2, which means that they have an exact numerical representation in a computer.

From the choice of values in (63), we compute $\psi_\pm$ and Υ in Section 5.2.2 using just double precision:

	ω_1	ω_2
ψ_-	2.468595425049463e − 01	2.093861593414215e − 01
ψ_+	2.682454746721682e − 01	2.306499653402554e − 01
Υ	1.833012143471895e − 06	1.842114896678543e − 06

Then, the Q quantities can be computed following Section 5.3. In this computation, we parallelize the different evaluations in a grid of $16 \times 16 \times 16$ points with a final CPU time of around 33 h with 31 threads and 18 h with 54 threads. As in the solution computed in Section 4.7, we perform all the computations with 170 bits of precision. In particular, we know that the error in the invariance equation, the ε_0 in Theorem 4.6, is at most 10^{-45} because it is the requested tolerance in the Newton's process. Moreover, once all the Q quantities are computed, we perform the final checks of inequalities (26)–(35) using a little bit more bits, say 250, to prevent possible overflows in the comparisons.

We conclude by saying that the conditions of the theorem are satisfied for the values given in (50) for ω_1 and (51) for ω_2. The values of the quantities needed to prove Theorem 4.6 for ω_1 and ω_2 are listed, respectively, in Appendix D and E. The values of ε that we obtain are essentially coinciding with the numerical break-down values, which are computed in [28]. This result shows the efficacy of KAM theorem in providing a constructive method to follow the invariant attractors up to break-down.

Declaration of competing interest

The authors declare that they have no known competing financial interests or personal relationships that could have appeared to influence the work reported in this paper.

Appendix A. List of the constants of Theorem 4.6

The explicit expressions of the constants used in Theorem 4.6 are given below (see [15] for their derivation).

$$\begin{aligned} C_{\sigma 0} &:= \mathcal{T}_0 \left[|\lambda - 1| \left(\frac{1}{\| \lambda| - 1|} \|S_0\|_{\rho_0} + 1 \right) + \|S_0\|_{\rho_0} \right] \|M_0^{-1}\|_{\rho_0} \,, \\ C_{W_2 0} &:= \frac{1}{\| \lambda| - 1|} \Big(1 + C_{\sigma 0} Q_e \Big) \|M_0^{-1}\|_{\rho_0} \,, \\ \overline{C}_{W_2 0} &:= 2\mathcal{T}_0 \left(\frac{1}{\| \lambda| - 1|} \|S_0\|_{\rho_0} + 1 \right) Q_e \, \|M_0^{-1}\|_{\rho_0}^2 \,, \\ C_{W_1 0} &:= C_0 \Big(\|S_0\|_{\rho_0} (C_{W_2 0} + \overline{C}_{W_2 0}) + \|M_0^{-1}\|_{\rho_0} + Q_e \|M_0^{-1}\|_{\rho_0} C_{\sigma 0} \Big) \,, \\ C_{W 0} &:= C_{W_1 0} + (C_{W_2 0} + \overline{C}_{W_2 0}) \nu \delta_0^\tau \,, \\ C_{\eta 0} &:= C_{W 0} \|M_0\|_{\rho_0} + C_{\sigma 0} \nu \delta_0^\tau \,, \\ C_{\mathcal{R} 0} &:= Q_{E 0} (\|M_0\|_{\rho_0}^2 C_{W 0}^2 + C_{\sigma 0}^2 \nu^2 \delta_0^{2\tau}) \,, \\ C_{\mathcal{E} 0} &:= C_{W 0} \nu \delta_0^{-1+\tau} + C_{\mathcal{R} 0} \,, \\ C_{d 0} &:= C_{W 0} \, \|M_0\|_{\rho_0} \,, \\ \kappa_e &:= 4 C_{\sigma 0} \,, \\ D_K &:= 4 C_{d 0} \, \nu^{-1} \delta_0^{-\tau-1} \, \varepsilon_0 \,, \\ D_{2K} &:= 4 \, C_{d 0} \nu^{-1} \delta_0^{-\tau-2} \, \varepsilon_0 \,, \end{aligned}$$

$$
\begin{aligned}
C_N &:= \|N_0\|_{\rho_0}^2 \ \frac{2\|DK_0\|_{\rho_0} + D_K}{1 - \|N_0\|_{\rho_0} D_K (2\|DK_0\|_{\rho_0} + D_K)} \ , \\
C_M &:= 1 + J_e \Big[C_N (\|DK_0\|_{\rho_0} + D_K) + \|N_0\|_{\rho_0} \Big] \ , \\
C_{Minv} &:= C_N (\|DK_0\|_{\rho_0} + D_K) + \|N_0\|_{\rho_0} + J_e \ , \\
C_S &:= 2 J_e Q_z \ \Big\{ (\|N_0\|_{\rho_0} + C_N D_K) \Big[D_K (\|N_0\|_{\rho_0} + C_N D_K) \\
&\quad + \|DK_0\|_{\rho_0} \|N_0\|_{\rho_0} + \|DK_0\|_{\rho_0} C_N D_K \Big] \\
&\quad + C_N \|DK_0\|_{\rho_0} \Big[D_K (\|N_0\|_{\rho_0} + C_N D_K) + \|DK_0\|_{\rho_0} \|N_0\|_{\rho_0} + \|DK_0\|_{\rho_0} C_N D_K \Big] \\
&\quad + \|N_0\|_{\rho_0} \|DK_0\|_{\rho_0} (\|N_0\|_{\rho_0} + C_N D_K) + C_N \|N_0\|_{\rho_0} \|DK_0\|_{\rho_0}^2 \Big\} \ , \\
C_{SB} &:= \frac{1}{\| \lambda| - 1|} Q_e \|M_0^{-1}\|_{\rho_0} C_S + 2 J_e Q_z \ \|N_0\|_{\rho_0}^2 \ \|DK_0\|_{\rho_0}^2 \frac{1}{\| \lambda| - 1|} \ C_{Minv} \ Q_e \\
&\quad + 2 C_S \ \frac{1}{\| \lambda| - 1|} \ C_{Minv} \ Q_e \ D_K \ , \\
C_\tau &:= \max \Big\{ C_S, C_{SB} + 2 C_{Minv} Q_e \Big\} \ D_K \ , \\
C_T &:= \frac{\mathcal{T}_0^2}{1 - \mathcal{T}_0 C_\tau} \ \max \Big\{ C_S, C_{SB} + 2 C_{Minv} Q_e \Big\} \ , \\
C_\sigma &:= C_T \ \Big\{ |\lambda - 1| \ \Big[\frac{1}{\| \lambda| - 1|} (\|S_0\|_{\rho_0} + C_S D_K) + 1 \Big] \\
&\quad + \Big(\|S_0\|_{\rho_0} + C_S D_K \Big) \Big\} \ \Big(\|M_0^{-1}\|_{\rho_0} + C_{Minv} D_K \Big) \\
&\quad + \mathcal{T}_0 \ \Big\{ |\lambda - 1| \ \Big[\frac{1}{\| \lambda| - 1|} (\|S_0\|_{\rho_0} + C_S D_K) + 1 \Big] C_{Minv} \\
&\quad + |\lambda - 1| \ \frac{1}{\| \lambda| - 1|} \ \|M_0^{-1}\|_{\rho_0} C_S + C_S \Big(\|M_0^{-1}\|_{\rho_0} + C_{Minv} D_K \Big) + C_{Minv} \|S_0\|_{\rho_0} \Big\} \ , \\
\overline{C}_{W_2} &:= 4 C_T \ \Big[\frac{1}{\| \lambda| - 1|} (\|S_0\|_{\rho_0} + C_S D_K) + 1 \Big] \ Q_e (\|M_0^{-1}\|_{\rho_0} + D_K)^2 \\
&\quad + 4 \mathcal{T}_0 Q_e \ \frac{1}{\| \lambda| - 1|} C_S \ (\|M_0^{-1}\|_{\rho_0} + D_K)^2 \\
&\quad + 4 \mathcal{T}_0 \ Q_e \Big[\frac{1}{\| \lambda| - 1|} (\|S_0\|_{\rho_0} + C_S D_K) + 1 \Big] (D_K + 2\|M_0^{-1}\|_{\rho_0}) \\
C_{\mathcal{R}} &:= Q_{E0} \ \Big[(2 C_M \|M_0\|_{\rho_0} + C_M^2 D_K)(C_{W0} + C_W D_K)^2 + \|M_0\|_{\rho_0}^2 (C_W^2 D_K + 2 C_{W0} \ C_W) \\
&\quad + (C_\sigma^2 D_K + 2 C_{\sigma 0} C_\sigma) \nu^2 \delta_0^{2\tau} \Big] + C_Q \ \Big[(\|M_0\|_{\rho_0} + C_M D_K)^2 (C_{W0} + C_W D_K)^2 \\
&\quad + (C_{\sigma 0} + C_\sigma D_K)^2 \nu^2 \delta_0^{2\tau} \Big] \delta_0^{-1} \ , \\
C_{W_2} &:= \frac{1}{\| \lambda| - 1|} \ \Big[1 + 2 Q_e \|M_0^{-1}\|_{\rho_0} C_\sigma + 2 Q_e C_{\sigma 0} + 2 Q_e C_\sigma D_K \Big] \ , \\
C_{W_1} &:= C_0 \Big[\|S_0\|_{\rho_0} C_{W_2} + C_S C_{W_2 0} + C_S C_{W_2} D_K + \|S_0\|_{\rho_0} \overline{C}_{W_2} \\
&\quad + C_S \overline{C}_{W_2 0} + C_S \overline{C}_{W_2} D_K + 1 + 2 Q_e \|M_0^{-1}\|_{\rho_0} C_\sigma + 2 Q_e C_{\sigma 0} + 2 Q_e C_\sigma D_K \Big] \ , \\
C_W &:= C_{W_1} + C_{W_2} \nu \delta_0^\tau + \overline{C}_{W_2} \nu \delta_0^\tau \\
C_Q &:= \frac{1}{2} \ \max \Big\{ 1 + \sup_{z \in \mathcal{C}} |D^3 f_{e_0}(z)| \ \|DK_0\|_{\rho_0}^2 \delta_0^2 \\
&\quad + \sup_{z \in \mathcal{C}, e \in \Lambda, |e - e_0| < 2\kappa_e \varepsilon_0} |D_e D^2 f_e(z)| \ \|DK_0\|_{\rho_0}^2 \ \frac{C_{\sigma 0}}{C_{d0}} \delta_0^{\tau+2} \\
&\quad + \sup_{z \in \mathcal{C}} |D^2 f_{e_0}(z)| \ \|DK_0\|_{\rho_0} \ \delta_0 \\
&\quad + \sup_{z \in \mathcal{C}} |D^3 f_{e_0}(z)| \ \|DK_0\|_{\rho_0} \ 4 C_{d0} \nu^{-1} \delta_0^{-\tau+1} \varepsilon_0
\end{aligned}
$$

$$
\begin{aligned}
&+ \sup_{z\in\mathcal{C},e\in\Lambda,|e-e_0|<2\kappa_e\varepsilon_0} |D_eD^2f_e(z)|\ \|DK_0\|_{\rho_0}\ 4C_{\sigma 0}\delta_0\varepsilon_0\\
&+ \sup_{z\in\mathcal{C}} |D^2f_{e_0}(z)|\ \|D^2K_0\|^2_{\rho_0}\ \delta_0^2\\
&+ \sup_{z\in\mathcal{C},e\in\Lambda,|e-e_0|<2\kappa_e\varepsilon_0} |D_eDf_e(z)|\ \|D^2K_0\|_{\rho_0}\ \frac{C_{\sigma 0}}{C_{d0}}\nu\delta_0^{\tau+2}\\
&+ \sup_{z\in\mathcal{C}} |D^2f_{e_0}(z)|\ (\|DK_0\|_{\rho_0}+D_K)\ \delta_0\\
&+ \sup_{z\in\mathcal{C}} |D^3f_{e_0}(z)|\ (\|DK_0\|_{\rho_0}+D_K)4C_{d0}\ \nu^{-1}\delta_0^{-\tau+1}\varepsilon_0\\
&+ \sup_{z\in\mathcal{C},e\in\Lambda,|e-e_0|<2\kappa_e\varepsilon_0} |D_eD^2f_e(z)|\ (\|DK_0\|_{\rho_0}+D_K)\ 4C_{\sigma 0}\delta_0\varepsilon_0\\
&+ \sup_{z\in\mathcal{C}} |Df_{e_0}(z)| + \sup_{z\in\mathcal{C}} |D^2f_{e_0}(z)|\ (4C_{d0}\nu^{-1}\delta_0^{-\tau})\ \varepsilon_0\\
&+ \sup_{z\in\mathcal{C},e\in\Lambda,|e-e_0|<2\kappa_e\varepsilon_0} |D_eDf_e(z)|\ \kappa_e\varepsilon_0\ ,\\
&\sup_{z\in\mathcal{C}} |DD_ef_{e_0}(z)|\ \delta_0 + \sup_{z\in\mathcal{C}} |D^2D_ef_{e_0}(z)|\ \delta_0^2\ (\|DK_0\|_{\rho_0}+D_K)\\
&+ \sup_{z\in\mathcal{C},e\in\Lambda,|e-e_0|<2\kappa_e\varepsilon_0} |DD_e^2f_e(z)|\ \frac{C_{\sigma 0}}{C_{d0}}\nu\delta_0^{\tau+2}\ (\|DK_0\|_{\rho_0}+D_K),\\
&\sup_{z\in\mathcal{C},e\in\Lambda,|e-e_0|<2\kappa_e\varepsilon_0} |D_e^3f_e(z)|\ \frac{C_{\sigma 0}}{C_{d0}}\nu\delta_0^{\tau+2}\Big\}\ .
\end{aligned}
$$

Appendix B. Newton's algorithm

In this Section, we provide Newton's algorithm for finding an invariant attractor of the spin–orbit problem; the algorithm is fully detailed in [14].

Algorithm B.1 (*Newton's Method for Finding a Torus in the Spin–Orbit Problem*)**.**

- ⋆ `Inputs:` A fixed frequency ω, the conformally symplectic map P_e given in (4) for fixed values of the parameters ε and η. Initial values of the unknowns; the eccentricity e and the embedding $K:\mathbb{T}\to\mathbb{T}\times\mathbb{R}$.
- ⋆ `Output:` New K and e satisfying the invariance equation (21) up to a given tolerance.
- ⋆ `Notation:` If A is a function defined in $\mathbb{T}$, $\overline{A}:=\int_{\mathbb{T}}A$ and $A^0:=A-\overline{A}$.

1. $E\leftarrow P_e\circ K-K\circ T_\omega$ denote the components $E:=(E_1,E_2)$,
   $E_1\leftarrow E_1-\mathtt{round}(E_1)$.
2. $\alpha\leftarrow DK$.
3. $N\leftarrow(\alpha^t\alpha)^{-1}$.
4. $M\leftarrow\begin{bmatrix}\alpha & J^{-1}\alpha N\end{bmatrix}$.
5. $\widetilde{E}\leftarrow(M^{-1}\circ T_\omega)E$.
6. λ given in (11).
7. $P\leftarrow\alpha N$,
   $S\leftarrow(P\circ T_\omega)^tDP_e\circ KJ^{-1}P$,
   $\widetilde{A}\leftarrow M^{-1}\circ T_\omega D_eP_e\circ K$ denote the components $\widetilde{A}:=(\widetilde{A}_1,\widetilde{A}_2)$.
8. $(B_a)^0$ solving $\lambda(B_a)^0-(B_a)^0\circ T_\omega=-(\widetilde{E}_2)^0$,
   $(B_b)^0$ solving $\lambda(B_b)^0-(B_b)^0\circ T_\omega=-(\widetilde{A}_2)^0$.
9. Find $\overline{W}_2$, σ solving the linear system

$$
\begin{pmatrix}\overline{S} & \overline{S(B_b)^0}+\overline{\widetilde{A}_1}\\ \lambda-1 & \overline{\widetilde{A}_2}\end{pmatrix}\begin{pmatrix}\overline{W}_2\\ \sigma\end{pmatrix}=\begin{pmatrix}-\overline{\widetilde{E}_1}-\overline{S(B_a)^0}\\ -\overline{\widetilde{E}_2}\end{pmatrix}
$$

10. $(W_2)^0\leftarrow(B_a)^0+\sigma(B_b)^0$.
11. $W_2\leftarrow(W_2)^0+\overline{W}_2$.
12. $(W_1)^0$ solving $(W_1)^0-(W_1)^0\circ T_\omega=-(SW_2)^0-(\widetilde{E}_1)^0-(\widetilde{A}_1)^0\sigma$.
13. $K\leftarrow K+MW$,
    $e\leftarrow e+\sigma$.
14. Iterate from 1 until convergence in E with a prescribed tolerance $\tilde{\epsilon}$.

Appendix C. Complexification of a Fourier series

If $x:\mathbb{T}\to\mathbb{R}$ is a periodic and smooth mapping of period 1, it admits an Nth order truncated Fourier series with Fourier coefficients $\{x_k\}_{k=0}^{N-1}\subset\mathbb{R}$:

$$x(\theta)=\frac{x_0}{2}+\frac{x_{N/2}}{2}\cos(\pi N\theta)+\sum_{k=1}^{N/2-1}x_{2k}\cos(2\pi k\theta)+x_{2k+1}\sin(2\pi k\theta)\,. \tag{64}$$

For simplicity and easy notation we assume N to be an even positive integer in (64). The complexification process of the map x consists in lifting the spaces $\mathbb{T}$ and $\mathbb{R}$ to the complex numbers such that it coincides with x when it is restricted to the real values.

To make it simpler, it is convenient to extend the quantity of real numbers in (64) and make explicit the symmetry in the complex version. In other words, (64) is equivalent to

$$x(\theta)=x_0+2\sum_{k=1}^{N/2}(x_{2k}-\mathtt{i}x_{2k+1})e^{2\pi k\mathtt{i}\theta}+(x_{2k}+\mathtt{i}x_{2k+1})e^{-2\pi k\mathtt{i}\theta}$$

with $x_{N+1}=0$. Now, if $\rho>0$, then

$$x(\theta+\mathtt{i}\rho)=x_0+2\sum_{k=1}^{N/2}(x_{2k}-\mathtt{i}x_{2k+1})e^{2\pi k\mathtt{i}(\theta+\mathtt{i}\rho)}+(x_{2k}+\mathtt{i}x_{2k+1})e^{-2\pi k\mathtt{i}(\theta+\mathtt{i}\rho)},$$

which allows one to provide the Fourier coefficients $\{(x_{2k}\pm\mathtt{i}x_{2k+1})e^{\pm2\pi k\rho}\}$ making the initial real Fourier expression to a complex one.

Appendix D. KAM quantities for the frequency ω_1

We list below the quantities needed to implement Theorem 4.6 to get the existence of an invariant attractor with frequency ω_1.

$$\begin{aligned}
N &= 16384\,,\\
\varepsilon &= 1.16329636418771163677161126429485305596755313822 97\mathtt{e}-02\,,\\
\eta &= 10^{-3}\,,\\
e &= 3.16752868911748321071860845138656617615717849736 18\mathtt{e}-01\,,\\
\rho_0 &= 2^{-17}\,,\\
\delta_0 &= 2^{-20}\,,\\
\|DK\|_{\rho_0} &= 6.20769698390325640484383256507779124192148450023 00\mathtt{e}+00\,,\\
\|DK^{-1}\|_{\rho_0} &= 1.83281299572584498744600754082339230384347126900 96\mathtt{e}+05\,,\\
\|D^2K\|_{\rho_0} &= 1.16860899451134488588216517458875733746651260817 19\mathtt{e}+02\,,\\
Q_{E_0} &= 1.91323152647925761021651227886803830788084328796 26\mathtt{e}+00\,,\\
\|N\|_{\rho_0} &= 9.80511718084959816700351374697087991083659493252 48\mathtt{e}+00\,,\\
\|N^{-1}\|_{\rho_0} &= 1.01139464108998262278270560065947834123574011149 59\mathtt{e}+01\,,\\
\|S\|_{\rho_0} &= 5.72233218309362490914126437881036539382621052454 20\mathtt{e}+01\,,\\
\|E_0\|_{\rho_0} &= 5.73565597818574037649792819305531403981863377166 56\mathtt{e}-48\,,\\
\lambda &= 9.86893599230429650271160696235087491078993671345 35\mathtt{e}-01\,,\\
\|M\|_{\rho_0} &= 1.20409582500275601418177375982274134584170759079 98\mathtt{e}+01\,,\\
\|M^{-1}\|_{\rho_0} &= \|M\|_{\rho_0}\,,\\
\mathcal{T}_0 &= 9.98199490094402592289009247485349327712890164376 41\mathtt{e}+01\,,\\
8C_\sigma\|E_0\|_{\rho_0} &= 6.31254183221172695194586089935742360311754833175 08\mathtt{e}-42\,,\\
\zeta &= 2^{-30}\,,\\
Q_z &= 6.61013000162094231954239755472392581764328518024 52\mathtt{e}+00\,,\\
Q_e &= 1.41758997117792931563632755370047566047990080986 06\mathtt{e}-01\,,\\
Q_{zz} &= 2.77208437111013916489709261562059525472961696751 64\mathtt{e}+01\,,\\
Q_{ez} &= 1.89537478093856775446887396349541940306624396854 38\mathtt{e}+00\,,\\
Q_{zzz} &= 1.07247653981152625970368155618283248533428467878 22\mathtt{e}+03\,,
\end{aligned}$$

$$
\begin{aligned}
Q_{ezz} &= 3.57492179937175419901227185394277495111428226260 74e+02\,,\\
Q_{ze} &= 1.89537478093856775446887396349541940306630822590 39e+00\,,\\
Q_{ee} &= 5.06628179167432595722060580328983983369854963052 33e-01\,,\\
Q_{zze} &= 3.57492179937175419901227185394277495111433168051 87e+02\,,\\
Q_{eez} &= 6.56472935042047765208160155024779829079618931780 51e+01\,,\\
Q_{eee} &= 1.14766575925368901598712661068146651459407574441 59e+00\,.
\end{aligned}
$$

Appendix E. KAM quantities for the frequency ω_2

We list below the quantities needed to implement Theorem 4.6 to get the existence of an invariant attractor with frequency ω_2.

$$
\begin{aligned}
N &= 4096\,,\\
\varepsilon &= 1.26976300244158830321238300136676135090099508261 68e-02\,,\\
\eta &= 10^{-3}\,,\\
e &= 2.48247408235631659022271000918697704257319964500 84e-01\,,\\
\rho_0 &= 2^{-17}\,,\\
\delta_0 &= 2^{-20}\,,\\
\|DK\|_{\rho_0} &= 6.24013680929893685609399113904809487962133238848 72e+00\,,\\
\|DK^{-1}\|_{\rho_0} &= 9.76633430521060625998541145243413546483009579979 91e+04\,,\\
\|D^2K\|_{\rho_0} &= 1.25992621906332026795740038777512364786768498239 24e+02\,,\\
Q_{E_0} &= 3.72831838559249882599494739785984089082753423003 33e+00\,,\\
\|N\|_{\rho_0} &= 9.72198701021888050117107096531010751193871493147 34e+00\,,\\
\|N^{-1}\|_{\rho_0} &= 1.02244861557366660178134941962533914212242976768 66e+01\,,\\
\|S\|_{\rho_0} &= 5.65662907180090948850710458504175929948999249650 64e+01\,,\\
\|E_0\|_{\rho_0} &= 4.51109638298956253724780568552419161072405820633 54e-45\,,\\
\lambda &= 9.90125101488077613468162987725618915861749782612 38e-01\,,\\
\|M\|_{\rho_0} &= 1.20400136019978894913013082422833646952454207205 97e+01\,,\\
\|M^{-1}\|_{\rho_0} &= \|M\|_{\rho_0}\,,\\
\mathcal{T}_0 &= 6.05574742798025200665317873579195837379908625609 32e+01\,,\\
8C_\sigma\|E_0\|_{\rho_0} &= 2.97709317602744067787882887544827729910656442427 39e-39\,,\\
\zeta &= 2^{-30}\,,\\
Q_z &= 6.55921652519904064453693410616226171265712765782 25e+00\,,\\
Q_e &= 1.50838175122312039862930897326633866925823676658 97e-01\,,\\
Q_{zz} &= 2.70923967271276680819141261446700119299644723512 48e+01\,,\\
Q_{ez} &= 2.76069214974361698243559153459165075385679984077 21e+00\,,\\
Q_{zzz} &= 1.00027775860416201536651897201041936729935322713 33e+03\,,\\
Q_{ezz} &= 3.33425919534720671788839657336806455766451075711 11e+02\,,\\
Q_{ze} &= 2.76069214974361698243559153459165075387358608055 55e+00\,,\\
Q_{ee} &= 2.83952388023808050945072343856911155890674080707 88e-01\,,\\
Q_{zze} &= 3.33425919534720671788839657336806455769420373785 72e+02\,,\\
Q_{eez} &= 7.20629242268729942360283882524352968031690265679 68e+01\,,\\
Q_{eee} &= 5.77959065920948382409536938198467694519268481208 80e-01\,.
\end{aligned}
$$

Appendix F. Multivariate polynomials of degree 2

Let us consider a polynomial with d variables and degree 2, namely

$$
p(x) = p_0 + \sum_{|k|=1} p_k x^k + \sum_{|k|=2} p_k x^k, \qquad k \in \mathbb{N}^d, x = (x_0, \ldots, x_{d-1}) \tag{65}
$$

Table 1
Bijection encoding between the exponent x^k with $x = (x_0, \ldots, x_{d-1})$, $k = \boldsymbol{e}_i + \boldsymbol{e}_j$, $i \geq j$, where $\boldsymbol{e}_l = (0, \ldots, 1, \ldots 0)$ and the location on the array containing the terms p_k of (65).

	Monomial	Multi-index	Index
$\chi(1) = 1$	x_0^2	$\boldsymbol{e}_0 + \boldsymbol{e}_0$	0
$\chi(2) = 3$	$x_1 x_0$	$\boldsymbol{e}_1 + \boldsymbol{e}_0$	1
	x_1^2	$\boldsymbol{e}_1 + \boldsymbol{e}_1$	2
$\chi(3) = 6$	$x_2 x_0$	$\boldsymbol{e}_2 + \boldsymbol{e}_0$	3
	$x_2 x_1$	$\boldsymbol{e}_2 + \boldsymbol{e}_1$	4
	x_2^2	$\boldsymbol{e}_2 + \boldsymbol{e}_2$	5
$\chi(4) = 10$	$x_3 x_0$	$\boldsymbol{e}_3 + \boldsymbol{e}_0$	6
	$x_3 x_1$	$\boldsymbol{e}_3 + \boldsymbol{e}_1$	7
	$x_3 x_2$	$\boldsymbol{e}_3 + \boldsymbol{e}_2$	8
	x_3^2	$\boldsymbol{e}_3 + \boldsymbol{e}_3$	9
$\chi(5) = 15$	$x_4 x_0$	$\boldsymbol{e}_4 + \boldsymbol{e}_0$	10
	$x_4 x_1$	$\boldsymbol{e}_4 + \boldsymbol{e}_1$	11
	$x_4 x_2$	$\boldsymbol{e}_4 + \boldsymbol{e}_2$	12
	$x_4 x_3$	$\boldsymbol{e}_4 + \boldsymbol{e}_3$	13
	x_4^2	$\boldsymbol{e}_4 + \boldsymbol{e}_4$	14

with the multi-index conventions $|k| = k_0 + \cdots + k_{d-1}$ and

$$x^k = x_0^{k_0} x_1^{k_1} \cdots x_{d-1}^{k_{d-1}}. \tag{66}$$

Note that in the case of degree 2, the multi-index k can be encoded with the canonical vector $\underline{e}_l = (0, \ldots, 1, \ldots, 0)$ with $0 \leq l < d$ in $\mathbb{R}^d$. That is, either $\underline{e}_i$ for $|k| = 1$ or $\underline{e}_i + \underline{e}_j$ with $i \geq j$ for $|k| = 2$.

Let us now define $\chi(i) = \#\{k \in \mathbb{N}^i : |k| = 2\}$, which is computable by the recurrence

$$\begin{aligned} &\chi(0) = 0, \\ &\chi(i) = \chi(i-1) + i, \quad i \geq 1. \end{aligned} \tag{67}$$

Thus the number of elements to store in a computer for (65) is $\chi(d) + d + 1$.

The crucial operation for an arithmetic of elements like (65) is the product, in which the key step is the product of the two homogeneous polynomials of degree 1, since the other terms are just multiplications by the independent term of each of the polynomials involved. To this end, we must fix a monomial order to encode the physical index of each of the monomials of degree 2. Among all of them, we consider the reverse lexicographical order, which is illustrated in Table 1 up to 5 variables.

Thus, the location in the array corresponding to $k = \underline{e}_i + \underline{e}_j$ with $i \geq j$ is given by $\chi(i) + j$. We implement this procedure in the function `ex2pl(i,j)` given below.

On the other hand, to know the i and j for a given index l in the vector of coefficients, one first performs a binary search to know k such that $\chi(k) \leq l < \chi(k+1)$, then $i = k$ and $j = l - \chi(k)$.

A possible pseudo code to compute the product pq of two homogeneous polynomials p and q with d variables and of degree 1 can then be

```
int ex2pl(i,j): return chi(max(i,j)) + min(i,j)

void php1(d,p,q,flag,pq):
  if (flag==0) for (i = 0; i < chi[d]; i++) pq[i]=0
  for (i = 0; i < d; i++) for (j = 0; j < d; j++)
   pq[ex2pl(i,j)]+= p[i] * q[j]
```

Once the product of multivariate polynomials of degree 2 is clear, the other elementary operations such as division, power, trigonometric operations and hyperbolic trigonometric operations can be derived in a recurrence manner, see [29]. For instance, the division of $r(x) = p(x)/q(x)$ has the following terms

$$\begin{aligned} r_0 &= \frac{p_0}{q_0}, \\ r_k &= \frac{p_k - r_0 q_k}{q_0}, && |k| = 1\,, \\ r_k &= \frac{1}{q_0}\Bigg[p_k - r_0 q_k - \underbrace{\left(\sum_{|j|=1} q_j x^j\right)\left(\sum_{|j|=1} r_j x^j\right)}_{\text{call to the php1 function}}\Bigg], && |k| = 2\,. \end{aligned} \tag{68}$$

References

[1] Kolmogorov AN. On conservation of conditionally periodic motions for a small change in Hamilton's function. Dokl Akad Nauk SSSR (N.S.) 1954;98:527–30; Stochastic Behavior in Classical and Quantum Hamiltonian Systems (Volta Memorial Conf., Como, 1977). Lecture Notes in Phys., vol. 93, Berlin: Springer; 1979, p. 51–6, English translation.
[2] Arnol'd VI. Proof of a theorem of A. N Kolmogorov on the invariance of quasi-periodic motions under small perturbations. Russian Math Surveys 1963;18(5):9–36.
[3] Moser J. On invariant curves of area-preserving mappings of an annulus. Nachr Akad Wiss Göttingen Math-Phys Kl II 1962;1962:1–20.
[4] de la Llave R, González A, Jorba À, Villanueva J. KAM theory without action–angle variables. Nonlinearity 2005;18(2):855–95.
[5] de la Llave R. A tutorial on KAM theory. In: Smooth Ergodic Theory and Its Applications (Seattle, WA, 1999). Providence, RI: Amer. Math. Soc.; 2001, p. 175–292.
[6] Moser J. Convergent series expansions for quasi-periodic motions. Math Ann 1967;169:136–76.
[7] Broer HW, Huitema GB, Takens F, Braaksma BLJ. Unfoldings and bifurcations of quasi-periodic tori. Mem Amer Math Soc 1990;83(421). viii+175.
[8] Broer HW, Huitema GB, Sevryuk MB. Quasi-Periodic Motions in Families of Dynamical Systems. Order Amidst Chaos. Berlin: Springer-Verlag; 1996.
[9] Ciocci Maria-Cristina, Litvak-Hinenzon Anna, Broer Henk. Survey on Dissipative KAM Theory Including Quasi-Periodic Bifurcation Theory (H. Broer). London Mathematical Society Lecture Note Series, Cambridge University Press; 2005, p. 303–56.
[10] Calleja Renato C, Celletti Alessandra, de la Llave Rafael. A KAM theory for conformally symplectic systems: efficient algorithms and their validation. J Differential Equations 2013;255(5):978–1049.
[11] Celletti Alessandra, Chierchia Luigi. Quasi-periodic attractors in celestial mechanics. Arch Ration Mech Anal 2009;191(2):311–45.
[12] Massetti Jessica Elisa. Normal forms for perturbations of systems possessing a diophantine invariant torus. Ergodic Theory Dyn Syst 2019;39(8):2176–222.
[13] Stefanelli Letizia, Locatelli Ugo. Kolmogorov's normal form for equations of motion with dissipative effects. Discrete Contin Dyn Syst 2012;17(7):2561–93.
[14] Calleja Renato C, Celletti Alessandra, Gimeno Joan, de la Llave Rafael. A map reduction and KAM tori construction for the dissipative spin–orbit problem. J. Nonlinear Sci. 2021. in press.
[15] Calleja Renato C, Celletti Alessandra, de la Llave Rafael. KAM estimates for the dissipative standard map. CNSNS 2021. in press, https://arxiv.org/abs/2002.10647.
[16] Hénon M. Exploration numérique du problème restreint IV: Masses egales, orbites non periodiquE. Bull Astron 1966;3(1):49–66.
[17] Beletsky VV. Essays on the Motion of Celestial Bodies. Basel: Birkhäuser Verlag; 2001, Translated from the Russian by Andrei Iacob.
[18] Celletti Alessandra. Analysis of resonances in the spin–orbit problem in celestial mechanics: the synchronous resonance. I Z Angew Math Phys 1990;41(2):174–204.
[19] Celletti Alessandra. Stability and Chaos in Celestial Mechanics. Berlin: Springer-Verlag; 2010, published in association with Praxis Publishing, Chichester.
[20] Correia Alexandre CM, Laskar Jacques. Mercury's capture into the 3/2 spin–orbit resonance as a result of its chaotic dynamics. Nature 2004;429(6994):848–50.
[21] Wisdom J, Peale SJ, Mignard F. The chaotic rotation of Hyperion. Icarus 1984;58(2):137–52.
[22] Macdonald Gordon JF. Tidal friction. Rev Geophys Space Phys 1964;2:467–541.
[23] Peale SJ. The free precession and libration of Mercury. Icarus 2005;178(1):4–18.
[24] Hairer E, Nørsett SP, Wanner G. Solving Ordinary Differential Equations. I. Springer Series in Computational Mathematics, 2nd ed.. vol. 8, Berlin: Springer-Verlag; 1993, p. 99–117, Nonstiff problems..
[25] Jorba À, Zou M. A software package for the numerical integration of ODEs by means of high-order Taylor methods. Exp Math 2005;14(1):99–117.
[26] Figueras J-Ll, Haro A, Luque A. Rigorous Computer-Assisted Application of KAM Theory: A Modern Approach. Foundations of Computational Mathematics; 2017, p. 1123–93.
[27] Das S, Saiki Y, Sander E, Yorke JA. Quantitative quasiperiodicity. Nonlinearity 2017;30(11):4111–40.
[28] Calleja Renato C, Celletti Alessandra, Gimeno Joan, de la Llave Rafael. Breakdown threshold of invariant attractors in the dissipative spin–orbit problem. 2021, Preprint.
[29] Haro Àlex, Canadell Marta, Figueras Jordi-Lluís, Luque Alejandro, Mondelo Josep-Maria. The Parameterization Method for Invariant Manifolds. Applied Mathematical Sciences, vol. 195, Cham: Springer; 2016, From rigorous results to effective computations.